Order Number 9119674

Vibrational circular dichroism and normal coordinate analysis of alanine dipeptides and several deuterated isotopomers

Roberts, Gull-Maj Lilian, Ph.D.

City University of New York, 1991

U·M·I
300 N. Zeeb Rd.
Ann Arbor, MI 48106

A

VIBRATIONAL CIRCULAR DICHROISM AND NORMAL COORDINATE ANALYSIS OF ALANINE DIPEPTIDES AND SEVERAL DEUTERATED ISOTOPOMERS.

by

Gull-Maj Lilian Roberts

A dissertation submitted to the Graduate Faculty in Chemistry in partial fulfillment of the requirements for the degree of Doctor of Philosophy, The City University of New York.

1991

This manuscript has been read and accepted for the Graduate Faculty in Chemistry in satisfaction of the dissertation requirement for the degree of Doctor of Philosophy.

Dec 13, 1990
Date

Chair of Examining Committee

Dec. 13, 1990
Date

Executive Officer

Supervisory Committee

The City University of New York

Abstract

VIBRATIONAL CIRCULAR DICHROISM AND NORMAL COORDINATE ANALYSIS OF ALANINE DIPEPTIDES AND SEVERAL DEUTERATED ISOTOPOMERS.

by

Gull-Maj Lilian Roberts

Adviser: Professor Max Diem

Normal coordinate analysis was carried out for the dipeptides L-alanyl-L-alanine, L-alanyl-D-alanine, and several deuterated isotopomers, in the spectral region above 1200 cm^{-1}. A Urey-Bradley force field was used in the calculations. The results were used for the interpretation of vibrational circular dichroism (VCD) spectra of the same species. The peptide model N-acetyl-L-alanine-N'-methylamide was also investigated using the VCD technique.

TABLE OF CONTENTS

TABLES

ILLUSTRATIONS

CHAPTER I

INTRODUCTION

Historical Background.

In 1812 the French physicist Jean Baptiste Biot carried out a series of experiments in which he shone white plane polarized light through a quartz plate and observed the emerging light through a second polarizer. He made the following observations: the light observed through such an arrangement is colored; the color depends on the orientation of the polarizers and on the thickness of the quartz plate; and when observing the same thickness of the two types of quartz known, complementary colors are observed for the same positions of the polarizers (right handed and left handed quartz can be distinguished by the shape of the crystal). Biot was thus the first scientist *to observe and describe the phenomenon of optical activity, in the form of optical rotatory dispersion. Further experiments with organic liquids and vapor of turpentine convinced him that the new property observed is not merely a property of an aggregation of molecules, but is, at least in some cases, a property belonging to the individual molecule. This was confirmed in 1850 when Louis Pasteur presented him with mirror image crystals of

tartrate, which when dissolved in water and analyzed, showed the same complementary behavior that Biot had observed for the two kinds of quartz crystal (1). These observations immediately raise two questions: What property of the material is responsible for the observed phenomenon, and what is the role of the light in these observations. The answers to these questions lead to a discussion of chiral molecules or aggregates, and to a description of circularly polarized light. To this might be added a third question: How may useful information be deduced from the observation of optical activity. The answers to this question lead to the development of the theory of optical activity, and to the different chiroptical techniques.

Chirality.

All optically active molecules have one property in common: They exist in a form which is non-superimposable on its mirror image. Thus the molecule and its mirror image have a relationship to each other much as our two hands, and the property has been named chirality (from the Greek word for hand). Some molecules exist naturally in both forms, which are said to be enantiomers of each other, others do not. In terms of symmetry chiral molecules are dissymmetric: They are either totally asymmetric and thus possess no symmetry elements, or they have one or more axes of proper rotation. Stated differently,

chiral molecules have no axes of improper rotation (2). A common example of an asymmetric molecule is a central carbon bonded to four different substituents (Figure 1, a). Any molecule containing such a group is chiral, its chirality originating in the carbon, which is called the chiral center. A common example of a chiral molecule which does not possess a chiral center is disubstituted allene which has axes of proper rotation (Figure 1, b).

An important group of large optically active molecules are those which form helices. Seen "from afar" these helical arrangements resemble springs and therefore possess axes of proper rotation. This means that identical units linked together and arranged as a helix will show overall chirality, even if each individual unit is not chiral. It is interesting in this context to consider that quartz consists of SiO_2 molecules, which are symmetric; yet in the crystal the molecules align themselves in a helical pattern, with the helix sense either clockwise or anticlockwise in a particular crystal, and the crystals are therefore optically active. Similarly, the simplest of the amino acids, glycine, has no chiral center. Polyglycine, however, may exist in the form of a helix and is therefore chiral by virtue of its overall spatial arrangement. It is interesting that in his early observations of optical activity Biot should have ob-

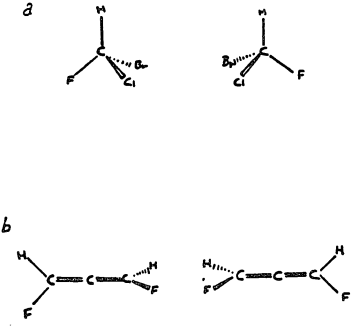

Figure 1. a) Bromochlorofluoromethane, an asymmetric molecule. b) 1,3 difluoroallene, a dissymmetric molecule with two axes of proper rotation. In each case both enantiomers are shown.

served molecules which are chiral because of their spatial arrangement as well as those whose chirality is inherent in the molecular structure.

Moving to molecules of some size and complexity - and that certainly applies to biological molecules - it soon becomes obvious that dissymmetry is the rule rather than the exception. Furthermore, nature has overwhelmingly favored one enantiomer over the other: naturally occurring proteins are made up almost entirely of one of the enantiomers of amino acids, the L-enantiomer. Any information which may be derived from the study of optical activity is therefore potentially of great interest and use to the study of biochemistry, molecular biology, and pharmacology. (L indicates levorotatory: The plane of the polarized light is turned to the left, or anticlockwise, in an optical rotation experiment. Clockwise rotation is denoted D for dextrorotatory).

Knowing the molecular property responsible for the observed optical activity, however, only partly explains why the observation is possible. The other part of the explanation comes from the answer to the question: What property of light allows us to distinguish between the two enantiomers of a chiral molecule?

Circularly Polarized Light.

The wave description of light describes plane polarized light as light in which the plane of the electric

vector is constant but its magnitude varies sinusoidally (Figure 2). In a similar manner one may describe a light wave in which the magnitude of the electric vector is constant, but the direction varies in such a way that the tip of the electric vector goes through a helical path, as seen by an imaginary observer standing in the path of the light and looking towards the source. (Figure 3) This is circularly polarized light, named right or left circularly polarized depending on whether the electric vector sweeps out a circle in the clockwise or anticlockwise direction (3). It is intuitively easy to accept that "chiral light" of opposite sense should interact differentially with a chiral molecule, and it will be shown in a later chapter that the phenomenon of optical activity indeed results from the interaction of a molecule (or molecular aggregation) with circularly polarized light.

To explain how optical activity may be observed using plane polarized light, as was done by Biot, it must be recognized that plane polarized light may be decomposed into two circularly polarized waves turning in opposite directions and going through one full revolution as the plane wave goes through a full wave. If these circular waves travel through a medium at different speeds (as expressed by the differential refractive index for left and right circularly polarized light) the resulting wave

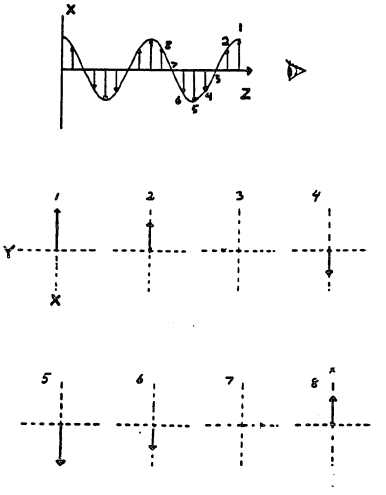

Figure 2. The wave description of light, showing the electric vector only. The top shows the traditional view, seen from the y-direction. The bottom shows the electric vector viewed from the direction of propagation, at different points in the cycle. As indicated the electric vector varies in magnitude, but not in direction.

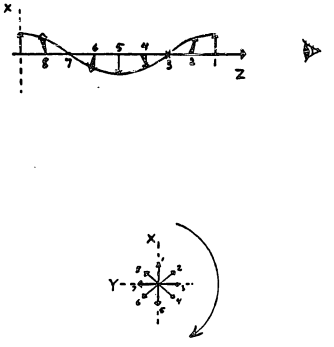

Figure 3. Right circularly polarized light. The top shows the propagation of light as seen from the y-direction; the bottom shows the instantaneous position of the electric vector as seen from the direction of propagation. As shown the magnitude of the electric vector is constant, but its direction varies with time.

will still be plane polarized but the orientation of the plane will have changed. This is the effect known as optical rotation. The angle through which the plane has turned will depend on the thickness of material traversed, or in the case of solutions, on the concentration and the pathlength. If the incoming light is a mixture of all the visible frequencies of light, namely white light, the orientation of the polarization plane will be different for each frequency as a result of variation of the refractive index over the frequency range. Thus a different color will dominate at each angle of rotation of the second polarizer, resulting in the optical rotatory dispersion observed by Biot.

Chiroptical Techniques.

The different chiroptical techniques all measure in various ways the differential interaction of right and left circularly polarized light with a medium. There are three commonly made measurements of interest in the context of this thesis (4).

1) Optical rotatory dispersion, ORD, measures the difference in the refractive index as a function of wavelength

$$\Delta n = n_L - n_R$$

where n is the refractive index, and the subscripts L and R stand for left and right circularly polarized light.

2) Raman Optical Activity, ROA, measures the differential scattering

$$\Delta I = I_L - I_R$$

The experiment is a modification of conventional Raman for measuring vibrational optical activity.

3) Circular dichroism measures the differential absorption

$$\Delta E = E_L - E_R$$

This effect can be observed in the UV-visible (CD), as well as in the infrared region (VCD). In analogy with regular UV-visible and IR spectroscopy the former probes the electronic and the latter the vibrational transitions.

ROA is mentioned here primarily because it, like VCD, probes the vibrational transitions. In analogy with conventional Raman and IR, it provides a technique complementary to VCD, but there have been substantial problems in the application of the technique, and it will not be discussed further here.

The Development of Vibrational Circular Dichroism.

In the development of chiroptical spectroscopy there has been a constant interplay between technology, theory and experimentation (4 - 6). Early discoveries such as Biot's were possible because of the discovery of natural-

ly occurring calcite crystals, which are uniaxial and therefore birefringent. It was discovered that a polarizer can be made of calcite when it is cut a certain way (3). As indicated earlier optical rotatory dispersion is a fairly simple technique which does not put great demands on instrumentation. The other techniques, however, are more demanding. In CD, for example, the effect measured is very small, typically 10^{-4} - 10^{-5} of the absorption. The main obstacle has therefore always been the detection of the signal and, as a consequence electronic CD was developed first. This technique has been helpful for elucidating the overall conformation of biomolecules since the early sixties. Thus the various polypeptide conformations, α helices, β sheets, and so forth, are associated with typical electronic CD signals.

Electronic CD, however, is limited by its dependence on the presence of a chromophore, a bond which will give rise to one of the electronic transitions measurable in the UV-visible region, and the number of such chromophores are limited. By contrast there are 3N - 6 possible vibrational sources of optical activity in the infrared region, corresponding to the 3N - 6 vibrational transitions. The information gained can also be expected to be different, since the electronic transition is fairly delocalized (because the electron involved is in the

excited state), whereas the vibrational transition takes place in the electronic ground state and arises from the motion of the nuclei. Thus it is related more directly to the structure and conformation of the molecule. It is therefore not surprising that there has been considerable interest in extending the scope of the CD technique to include the vibrational region. Early attempts at demonstrating the possibility of measuring the CD signals in this region were theoretical papers, which extended the knowledge gained in electronic CD to predicting signals in the vibrational region. Of these the calculations by Deutsche and Moscowitz introduced the fixed partial charge model, which predicted the VCD spectrum of a helical polymer (7, 8). Schellman and coworkers wrote several papers showing that the experience gained in electronic CD could be used in the calculation of vibrational CD spectra, and made suggestions of suitable molecules (9 - 12). Thus, using a similar model to the one developed by Deutsche and Moscowitz, Schellman calculated the expected VCD spectra of optically active cyclic amides, and predicted that the signals would be of comparable magnitude to those observed in electronic CD (9). At about the same time Holzwarth and Chabay developed the coupled oscillator model (13) in analogy with work done by Tinoco for electronic CD (14). They, too, suggested specific molecules (diketopiperazines) as good candidates

for measuring the weak effect.

Besides the general improvement of conventional infrared spectrometers over the years there are three specific developments which have been crucial to the development of VCD instruments: semiconductor detectors, which have higher sensitivity and faster response time than conventional detectors, the double modulation technique for extracting a signal smaller than the surrounding noise, and modulators for producing rapidly alternating left and right circularly polarized light (15). Semiconductor detectors can be made from a range of materials with different dopants, with the result that the range covered by these detectors has continued to expand. Thus early VCD experiments were made using InSb detectors with a range from approximately 1000 to 2000 cm^{-1}. Later HgCdTe detectors have extended that range to around 500 cm^{-1}, so that the instrumental cutoff is determined by other elements along the optical path, such as the lenses used. The range in which the detector is working at its maximum capacity can be varied in the manufacture by varying the proportions of the dopants. This has added great flexibility whereby the instrument now can be optimized for a particular range. The area of the detection element has also been increased, allowing for more efficient light collection.

The high frequency polarization modulation technique developed by Grosjean and Legrand (16, 17) has made it possible to increase the sensitivity of the detection of left versus right circularly polarized light by at least two orders of magnitude. The signal is modulated twice, first by a conventional mechanical chopper and then by sending the previously plane polarized light through a crystal, in which the birefringence is modulated either by mechanical stress (photoelastic modulator, or PEM), or by an applied voltage (electro-optic modulator, or EOM) (18). This technique also relies heavily on the availability of sophisticated lock-in amplifiers, which detect the differential interaction of the two circularities, at the modulation frequency.

The first eagerly anticipated measurements of VCD signals were reported by several groups in 1972 - 73 for liquid crystals (19 - 22), and were soon followed by measurements of single crystals (23) and neat liquids (24). This was followed in 1975 and '76 by three papers by Stephens's group, which not only demonstrated that the new technique could be applied to many compounds but also provided suggestions for instrumental improvements; they did not, however, try to interpret the results (25 - 27). Stephens and his coworkers have continued to work with VCD: Keiderling and his group have primarily made measurements on polypeptides and other protein-like systems,

in solutions as well as in thin films; Nafie's group has concentrated on smaller peptides and amino acids, while also spending considerable efforts on the development of new models. They have also built an instrument and developed the theory for FT-VCD. Meanwhile Stephens's group has mainly concentrated on theory and has developed a successful method for making ab initio calculations of VCD transitions. The method, like most of its kind, is computer intensive and can so far only be carried out on small molecules (See reference 4 for review of early work, and reference 5 for review of more resent work done in the field).

Our group, led by Max Diem, originally worked on instrumental design with special interest in the mid infrared region where most of the peptide modes occur, with the specific intention of studying small peptides in aqueous solution. This work has recently been expanded to include work on DNA.

Arrangement and Scope of this Thesis.

It has long been accepted that the three dimensional structure of an enzyme is a key to understanding its activity. Moreover, the enzyme substrates are often small strands of peptides, which take up specific conformations when interacting with the enzyme. Such relatively small biomolecules are ideal candidates for VCD studies. The

efforts of this group in that context has been to build up a detailed understanding of the conformation of small peptides in aqueous solution, using the technique of vibrational circular dichroism in conjunction with conventional Raman and IR spectroscopy, and starting with such simple molecules as alanyl-alanine and the peptide model N-acetyl-L-alanine-N'-methylamide (AAMA). The first part of my thesis forms the background of this understanding as it deals with the vibrational analysis and the normal coordinate calculations of alanyl-alanine, which were considered necessary for the proper interpretation of the VCD spectra.

Early efforts at collecting Raman spectra of peptides revealed that certain regions of the spectrum show sensitivity to the conformation of the peptide, in particular the regions known as the amide I and amide III regions. These regions, which lie around 1700 cm^{-1} and 1300 cm^{-1} respectively, have therefore become our main focus of interest. Of these the amide III vibrations were not clearly understood, and the first task was therefore considered to be the thorough examination of the amide III region of the simplest possible chiral peptide, alanyl-alanine. Earlier studies of alanine show that the methine deformations fall in this region (28); it was therefore a reasonable assumption that the amide III vibrations should involve these deformations, as well as

the deformations the N-H hydrogen of the peptide linkage. To sort out the possible contributions of the various modes involved it was decided to synthesize a series of isotopically substituted alanyl dipeptides which had one or both of the methine hydrogens exchanged with deuterium. Chapter II explains how the necessary peptides were synthesized, using the Merrifield method of synthesis. The Raman study of the synthesized peptides was done by other members of this group and will therefore not be described in detail here (29). However, the results of that study are so closely intertwined with the setting up and interpretation of the normal coordinate analysis that they will be carefully explained at the beginning of chapter IV. Chapter III gives the theory of the normal coordinate analysis and introduces the computer programs used in the calculations. Chapter IV, as already indicated, explains the normal coordinate calculations, defines what criteria were used for choosing the force field, and interprets the results.

The topic of the second part of this thesis is the VCD studies of the alanine dipeptides and of N-acetyl-L-alanine-N'-methylamide, AAMA. Thus chapter V starts with an explanation of the theory of VCD, and of the many models which have been developed. The coupled oscillator model is described in detail. This is followed by a

chapter which gives a detailed description of the VCD instrument used at Hunter college. Chapter VII is an account of the VCD studies of the same isotopically substituted species which were examined via vibrational analysis in chapters III and IV. Finally, Chapter VIII is a short chapter about the VCD results obtained for AAMA, stating developments so far and pointing to possible further studies. The four chapters of the second half of the thesis will hopefully give an impression of the complexity of the VCD spectra, and of the difficulties encountered in obtaining and interpreting them, as well as of the potential usefulness of this still fairly new technique.

CHAPTER II

SYNTHESIS OF ALANYL-ALANINE ISOTOPOMERS.

The Merrifield Method of Peptide Synthesis.

Peptides are synthesized, in nature as well as in the laboratory, by the addition of one amino acid to the next, accompanied by the loss of one water molecule:

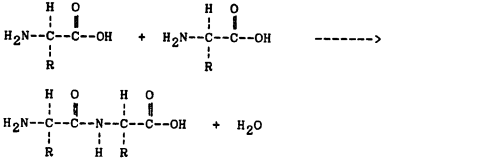

The method employed by us in synthesizing peptides is based on the method developed in the 1960s by R. B. Merrifield, known as the Merrifield Method of solid phase peptide synthesis (30). Until then peptide synthesis had been carried out in solution, which had one serious drawback: the new peptide obtained after each addition of an amino acid had to be isolated and purified (recrystallized). The result was that the yield after each successive addition became smaller, so that the synthesis of long peptide chains became just about impossible. Merrifield solved the problem in the following manner: the C-

terminal of the first amino acid is anchored to a solid support, a resin bead, via a benzyl ester linkage. The other end of the amino acid, the N-terminal, is protected by some bulky end group. The synthesis proceeds by successively removing the protection group and adding the next amino acid with its protection group already in place. These two steps are repeated until the chain has the desired length, after which the whole chain is cleaved off the resin. Notice that the synthesis proceeds from the C-terminal towards the N-terminal of the peptide: the opposite of the way it is usually written. Using this method the various reagents and solvents are simply washed away, once they have served their purpose, leaving the growing peptide firmly anchored to the resin. The purity of the product depends only on the complete removal of the protection group and the success of the addition of the next amino acid.

Outline of the Synthesis.

The vibrational analysis of alanyl-alanine required that a number of isotopically substituted species were available. The easiest way of obtaining an isotopomer is to dissolve the parent molecule in D_2O, stir the solution well and evaporate off the solvent. This exchanges all the labile protons with deuterium:

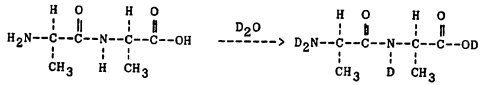

L-alanyl-L-alanine

L-alanyl-L-alanine, labile protons exchanged.

The remaining protons are the methyl hydrogens and the methine hydrogen, one set for each amino acid. Of these only the methine hydrogens were thought to have any contribution in the region of special interest, the amide III region. We therefore synthesized two dipeptides with the methine deuterated, which yielded two more isotopomers when they were dissolved in D_2O:

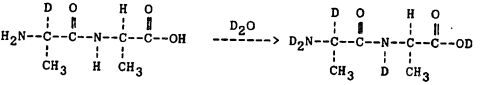

L-alanyl-d_1-L-alanine

L-alanyl-d_1-L-alanine, labile protons exchanged.

and

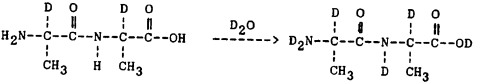

L-alanyl-d_1-L-alanine-d_1

L-alanyl-d_1-L-alanine-d_1, labile protons exchanged.

The synthesis consisted of six parts:

A) Deuteration of the methine position of the amino acid,

which proceeds with racemization.

B) Optical resolution to obtain the L-isomer.

C) Protection of the N-terminal.

D) Attachment of the first amino acid to the resin.

E) Synthesis of the dipeptides.

F) Cleavage of the peptide from the resin.

A) Deuteration of the Methine Proton in DL-alanine.

In a 4.5 g sample of DL-alanine all labile protons were exchanged by repeatedly dissolving in D_2O and subsequently evaporating to dryness. The sample was then dissolved in about 50 mL acetic anhydride, and 12 mL of D_2O was added. This was stirred for about two minutes, and another two mL D_2O was added. It was again stirred for two minutes and evaporated to dryness. The resulting compound was N-acetyl-LD-alanine-2-d_1.

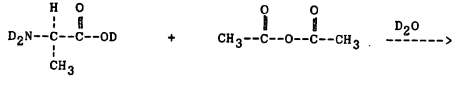

alanine acetic anhydride

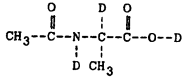

N-acetyl-LD-alanine-2-d_1

The completeness of this step was tested via NMR (60-MHz

Varian EM-360A Spectrometer): the quadruplet due to the methine and the doublet due to the methyl hydrogens on the chiral carbon collapse to one singlet (the unsplit methyl hydrogens) when the deuteration is complete. The chemical shift, δ, is 1.35 (for the acetyl methyl group, δ is approximately 2). Usually the procedure had to be repeated several times before deuteration was complete.

B) Resolution of N-acetyl-DL-alanine-2-d_1 (31).

The resolution of the two enantiomers was achieved by incubating an aqueous solution of pH 7.0 with Acylase I (Sigma Chemical Co.), 20 mg/13.1 g of sample, for 24 hours at 38° C. At the end of this time another batch of Acylase I was added, 5 mg /13.1 g, and the incubation was continued for another 16 hours (the exact time is not crucial). The acylase cleaves the L-enantiomer to L-alanine-2-d_1 and acetic acid but leaves the N-acetyl-D-alanine-2-d_1 uncleaved.

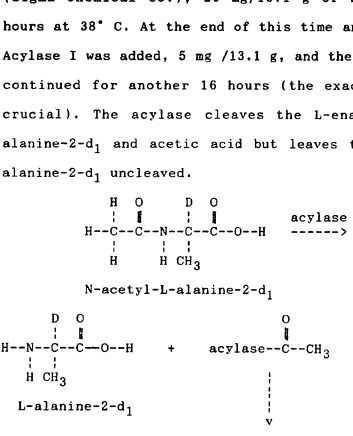

N-acetyl-L-alanine-2-d_1

L-alanine-2-d_1

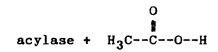

C) Protection of the N-terminal (32).

The protection group in this synthesis was a tert-butoxy group. It was attached to the N-terminal of the amino acid by treating this with di-tert-butyl-dicarbonate. 10 mmol of amino acid was dissolved in 50 mL of a 2:1 mixture of dioxane and water. While cooling in an ice bath 10 mL 1M NaOH was added. Following this, 11 mmol of di-tert-butyl-dicarbonate was added, and it was stirred for thirty minutes.

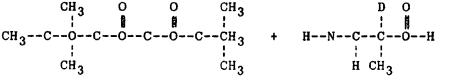

di-tert-butyl-dicarbonate L-alanine-2-d_1

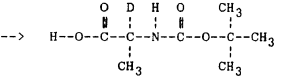

t-boc L-alanine-2-d_1

The sample, after evaporation, contained a mixture of t-boc-alanine-2-d_1 and unprotected amino acid. These were separated by dissolving the sample in ethyl acetate, acidifying with $KHSO_4$ to a pH of 2, and washing with water. The unprotected amino acid dissolved in the aqueous layer, but the protected did not.

D) Attachment of the first amino acid to the resin (33). The next step was to attach the first t-boc-alanine to the resin, which is an insoluble copolymer of styrene and divinyl benzene (Merrifield-resin), via a benzyl ester linkage. The method for doing this is cited in the reference. In the present case some resin had already been prepared by other members of the group.

E) Synthesis of the Dipeptides (30).

As already stated the Merrifield method of peptide synthesis starts with a single amino acid bonded to a resin bead at the C-terminal. The other end of the amino acid is protected by a tert-butoxy group (t-boc group). (In the following () indicates a hexane ring and (o) a benzene ring. The resin bead surface is indicated by ¦). The synthesizer used is depicted in Figure 1. The motor provides a rocking motion which effectively mixes the resin with any reagent. At the end of each step the synthesizer is drained into a reservoir, and the next reagent is added. Since the peptide is always bonded to the resin any by-products or impurities are simply washed away.

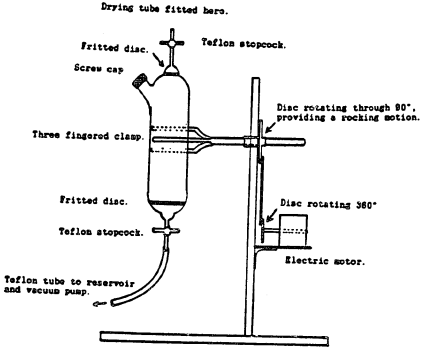

Fig.1. Peptide synthesizer. All parts of the synthesizer are either glass or teflon because of the triflouroacetic acid used in the synthesis. The flask is about 9 inches long and 2 inches in diameter.

Starting with

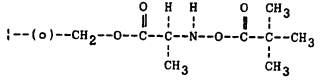

Resin 1st Ala t-boc

the peptide chain is built by 1) cleaving off the t-boc group (deprotection), and 2) adding the next amino acid, which is already protected with a t-boc group at the N-terminal.

1) The t-boc group is cleaved off using trifluoroacetic acid (TFA)

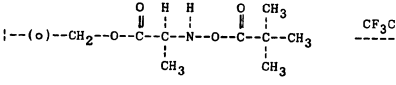

Resin 1st Ala t-boc

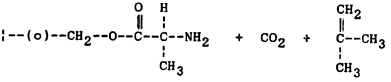

Resin 1st Ala isobutylene

2) The next Ala-t-boc is added with dicyclohexylcarbodiimide, (DCC). These form a reactive intermediate, which reacts with the amino acid on the resin.

i

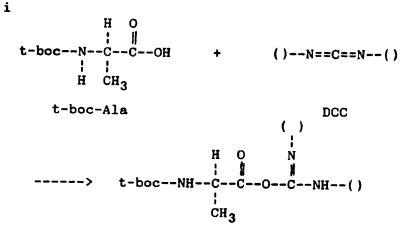

reactive intermediate

ii

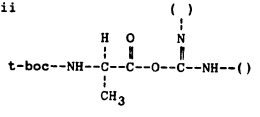

reactive intermediate

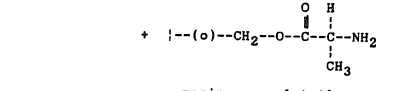

resin- 1st Ala

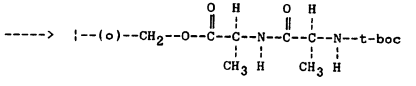

resin- 1st Ala- 2nd Ala- t-boc

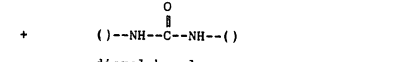

dicyclohexyl urea

Steps i and ii are repeated until the peptide chain has the desired length.

In order to end up with only one product, and avoid a mixture of peptides of different length and composition it is necessary to have a way of monitoring the success of each step. For this the ninhydrin test was used (34,35). This very sensitive test determines whether the last unit on the peptide chain is an amino group, that is, whether or not the last amino acid has a protection group at its N-terminal.

For the test three solution were prepared:

1) 500 mg ninhydrin in 10 mL ethanol.

2) 80 g phenol in 20 mL ethanol.

3) 2 mL 0.001 M KCN solution diluted with pyridine to make a 100 mL solution.

A very small sample of the resin is placed in a small test tube. To the test tube is added 2-3 drops of each of the prepared reagents, and the test tube is heated in a beaker of water to 100° C for about five minutes.

Positive result: The solution and the beads turn deep blue after two minutes heating, indicating the presence of free amines.

Negative result: The solution turns yellow or pale purple, but the beads have their original off-white color, indicating that no free amines are present.

It is very simple to see whether the test is positive but less obvious if it is definitely negative. Therefore a solution was usually made up of the reagents only, with no free amines present. Upon heating, this solution would turn yellow or pale purple, and served to show what a completely negative result should look like. However, the test is so sensitive to the presence of free amines that even with a slightly positive test (pale blue beads, trace blue solution) less than one percent of free terminal amines are present (34).

F) Cleavage of the Peptide from the Resin (36).

The resin was suspended in TFA in a round bottom flask, cooled in a mixture of water, ice and salt, and HBr gas was bubbled through for about an hour. The set-up is shown in Figure 2.

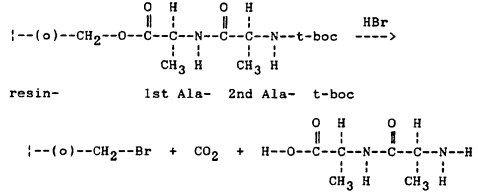

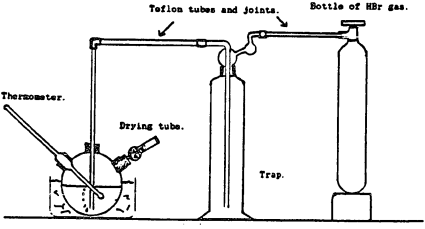

Figure 2. Apparatus for cleaving the peptide off the resin (in the hood). Since "back-pressure" is common the trap must be arranged so that no solvent can get into the HBr flask, which might otherwise explode. Everything must be securely clamped and all joints carefully checked for leaks.

The final purification of the peptide depends on its solubility. When making di- and tripeptides it has been sufficient to recrystallize the peptide from a water/acetone mixture, taking advantage of the fact that the peptides are very soluble in water but not in acetone.

Step by Step Reaction Scheme.

For non-deuterated samples the Merrifield resin is generally bought with the first amino acid already attached. 1 g of resin will give approximately 1 mmol of product. The synthesizer used works well with 2.5 g of resin, and could probably be used with 3 g. The quantities given here assume 2.5 g of resin.

#	Reagent	Vol.	# of times	Duration	Remarks
1	CH_2Cl_2	65mL	1 2 3	1 min	
2	50% TFA/CH_2Cl_2	65mL	1	2 min	TFA
3	50% TFA/CH_2Cl_2	65mL	1	40 min	Deprotection
4	CH_2Cl_2	65mL	1 2 3 4 5	1 min	
5	2-propanol	45mL	1 2	1 min	
6	CH_2Cl_2	65mL	1 2	1 min	

Ninhydrin test - should be positive					

7	5% DIEA*/ CH_2Cl_2	65mL	1	2 min	

8	CH_2Cl_2	65mL	1 2 3 4 5	1 min	
9	t-boc-Ala/ CH_2Cl_2	25mL	1	5 min	DO NOT DRAIN
10	DCC-CH_2Cl_2	25mL	1	50 min	Coupling
11	CH_2Cl_2	65mL	1 2 3 4	1 min	
12	2-propanol	45mL	1 2	1 min	
13	CH_2Cl_2	65mL	1 2 3 4 5	1 min	
14	2-propanol	45mL	1 2	1 min	
15	CH_2Cl_2	65mL	1 2 3	1 min	

Ninhydrin test - should be negative

---

* DIEA, diisopropyl ethyl amine, is a sterically hindered base:

Its purpose is to neutralize any remaining TFA.

For the coupling step 5 mmol of t-boc-Ala was used, that is twice as much as the expected yield. If this step needed repeating about half as much as the expected yield was used.

In conclusion it should be mentioned that Hunter College now has its own peptide synthesizing facility. However, the quantities made there are very small from a

spectroscopists point of view and it is often faster for us to make the small peptides ourselves.

CHAPTER III

NORMAL COORDINATE ANALYSIS: THEORY AND COMPUTATIONAL METHODS.

The Harmonic Oscillator Model of Molecular Vibrations.

The harmonic oscillator is one of the few systems for which the Schrödinger equation can be solved (37). This is significant because the vibrations of the nucleus of an atom in a molecule can be described in terms of such an oscillator. If we imagine the oscillations of the nucleus to be due to the stretching and contracting of a bond it can be seen that for small displacements about the equilibrium position the nucleus behaves very much like a mass attached to a spring. However, as the oscillations about the equilibrium position increase in amplitude the nucleus will at one extreme (contracting) meet with the repulsive force of the nucleus at the other end of the bond, and at the other extreme (expanding) feel less and less of the attractive force of the bond until the bond breaks and the molecule falls apart, Figure 1. Similar arguments hold for other motions of the nuclei. But for small displacements the motion is very similar to the harmonic oscillations of a mass attached to a spring, a system which is well described by classical mechanics. The calculations of the motion of the nuclei therefore begin with the classical picture.

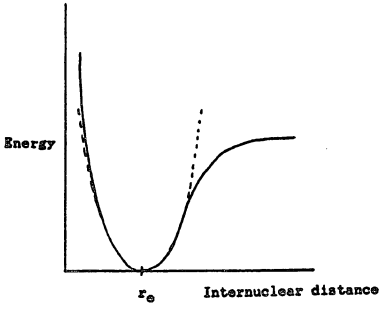

Figure 1. Example of a potential energy curve for two nuclei with equilibrium bond length r_e. The broken line indicates the energy of a harmonic oscillator. Close to the equilibrium, i. e., for small vibrations, the two curves coincide.

The Born-Oppenheimer Approximation.

When calculating the energies of the vibrations of the molecule we are assuming that the potential due to the electrons around each nucleus is constant in time and only varies as a function of the nuclear coordinates. Figure 1 is a pictorial description of the resulting "potential well" created by the electronic potential, in which the nucleus moves. This assumption is the Born-Oppenheimer approximation (38). Another way of stating it is to say that the electronic wavefunction and the nuclear wavefunction are separable. It means that for situations in which the approximation is valid it is possible to consider the vibrations of the nuclei without having to take into consideration the motion of the electrons.

Methods Used for Calculating the Vibrations of a Molecule.

In their book "Molecular Vibrations", Wilson, Decius and Cross developed a method for calculating the vibrations of small molecules which has proved to be very useful for spectroscopists (39). The method was originally developed to be used in connection with group theory - and therefore limited to molecules which possess some symmetry- but the use of computers, together with the development of fast algorithms for diagonalizing ma-

trices, has made it possible to carry out the calculations for any small molecule. The computer programs used to carry out the calculations based on Wilson's methods were developed by Schachtschneider (40) and later modified by Diem for use on a PC (41). The following will therefore be a brief account of the theory behind the method developed by Wilson, followed by an account of how the method is incorporated into the programs.

Theoretical Background.

As described in "Molecular Vibrations", chapter 2 we can express the kinetic energy, T, and potential energy, V, in mass weighted Cartesian coordinates, q_i, such that

$q_1 = \sqrt{m_1}\Delta x_1 \quad q_2 = \sqrt{m_1}\Delta y_1$, etc.,

where m is the mass of the atom and the Δ's indicate the atomic displacements from the equilibrium position. Furthermore, we can express the potential energy as a power series expansion, of which only one term is significant. This yields for the kinetic energy:

$$2T = \sum_{i=1}^{3N} \dot{q}_i 2 \qquad 1$$

and for the potential energy:

$$2V = \sum_{i,j=1}^{3N} f_{ij}\, q_i q_j \qquad 2$$

$$\text{where} \quad f_{ij} = \frac{\delta^2 V}{\delta q_i \delta q_j} \qquad 3$$

N is the number of atoms and $\dot{q}$ is the derivative of the displacement coordinate with respect to time. Using Newton's equation of motion in the following form

$$\frac{d}{dt}\frac{\delta T}{\delta \dot{q}_j} + \frac{\delta V}{\delta q_j} = 0$$

and substituting the values T and V, one gets

$$\ddot{q}_j + \sum_{i=1}^{N} f_{ij} q_{ij} = 0 \qquad j = 1, 2, \ldots 3N \qquad 4$$

which is a set of simultaneous second-order differential equations. The trial solutions to these are

$$q_i = A_i \cos (\lambda^{1/2} t + c) \qquad 5$$

When these solution are substituted in the differential equations a set of simultaneous homogeneous linear algebraic equations is obtained

$$\sum_{i=1}^{3N} (f_{ij} - \delta_{ij}\lambda) A_i = 0 \qquad j = 1,2,\ldots,3N \quad 6$$

where The δ_{ij} is the kronecker delta and the A_i's are the unknown amplitudes. To find the non-trivial solutions we set the determinant equal to zero (the secular equation). The solution to this gives a set of values for λ for

which the A_i's are non-zero, that is for each λ_k there are corresponding A_{ik}'s. The amplitudes are not uniquely determined in that only the relative amplitudes are known.

Interpretation of the Results of the Solutions to the Harmonic Oscillator.

We have obtained a set of solutions to Newton's equation of motion (equation 3 and 4) via the trial solution

$$q_i = A_i \cos(\lambda^{1/2}t + c) \qquad 5$$

for which we now have the frequencies, given by $\lambda^{1/2}/2\pi$, the relative amplitudes and the relative displacements of the vibrations of the atoms in a molecule. There are 3N solutions corresponding to the 3N roots to the set of algebraic equations. Six of these are zero as they correspond to the three rotational and the three translational motions of the molecule. The remaining 3N - 6 solutions correspond to 3N - 6 frequencies at which the molecule can vibrate (3N - 5 for linear molecules). For each frequency, corresponding to each λ, the relative displacements of the coordinates are given by the amplitudes, A_i. This simultaneous motion of all the atoms at the same frequency and in phase is known as a normal mode. Although the absolute amplitudes are not known the relative amplitudes show which motion or motions are the main contributors to a particular normal mode. The normal

modes are usually named after their main contributor, such as "C-H stretch" or "N-H deformation" whenever that is possible. The calculations give no information about combination bands, overtones, selection rules or special effects, such as Fermi resonance, which are encountered in vibrational spectroscopy. Such information must be found from quantum mechanical considerations and from experimental data.

Normalization of the Amplitudes.

To give some numerical value to the amplitude of each λ calculated it is only necessary to arbitrarily fix the value of one. However, there is a more satisfactory way of dealing with this (39): The A_i's are first given arbitrary values, A'_i, by giving one of them the value 1. We can then define a term k_i such that

$$k_i = \frac{A'_i}{[\sum_i (A'_i)^2]^{\frac{1}{2}}} \qquad 7$$

This definition was chosen because

$$\sum_i k_i^2 = 1$$

The Normal Coordinates.

It is implied in the solution to the secular equation that there exists a set of coordinates, Q_k, such that

$$2T = \sum_{k=1}^{3N} \dot{Q}_k^2 \qquad \text{and} \qquad 2V = \sum_{k=1}^{3N} \lambda_k Q_k^2 \qquad 8$$

The Q_k's are the normal coordinates. The name refers to the fact that there is one coordinate associated with each normal mode of vibration.

Spectroscopy and Normal Coordinate Calculations.

It has been assumed in the above calculations that the potential energy is known, and in particular that for the significant term

$$2V = \overline{\sum} f_{ij} q_i q_j$$

the force constants, f_{ij}, are known (equation 3). This is almost never the case: when a normal coordinate analysis is carried out it is usually after all the vibrations have been assigned. The force constants are given values, usually from the results of other calculations of similar molecules or from ab initio calculations, and adjusted until the observed spectrum can be reproduced. The goodness of the force constants can then be ascertained by isotopic substitution; since the major difference between two isotopes is the difference in mass the potential field around them is assumed to be the same. Therefore the frequency shift observed due to isotopic substitution

should be due to the change in mass only, and the same potential energy should accurately predict the new frequencies. This implies that spectra must be collected for several isotopically substituted species of the molecule of interest, and the calculations carried out for all species, using the same force constants. In practice, therefore, the value of the calculations lie in the information they give about the displacement of the atoms and the nature of the potential field: this information is contained in the normal coordinates. Only under special circumstances can the calculated frequencies be used to settle uncertainties regarding an assignment.

As will be shown, the programs, which were developed to carry out the normal coordinate calculations, were written from the spectroscopist's point of view: it is easy to change the force constants and to check the calculated against the observed frequencies.

The Computer Programs.

The programs used for the normal coordinate calculations are adaptations of the programs developed by Schachtschneider (40). They have been modified for use on a PC which has been equipped with a mathematics coprocessor (41). There are four programs: CART, BMAT, UBZM, and NOCO, which will be discussed next. In the text boldface type is used to indicate that the quantity is a matrix,

since most of calculations are made via matrices. To indicate the transpose of a matrix the superscript t is used.

CART

In CART the geometry of a molecule is input using only the positions of the atoms defined by bond lengths and bond angles. The program calculates the atomic positions in a Cartesian coordinate system which has its origin in the first atom defined and its positive x-axis along the first bond defined. The second bond defines the x-y plane and the positive y direction. The positive z-axis is defined by the first atom which is not lying in the x-y plane.

BMAT

The program BMAT transforms internal coordinates to Cartesian coordinates. The possible motions of a molecule are most easily defined as displacements of the atoms along a set of internal coordinates, **R**, which here are

a) bond stretches
b) deformations of bond angles
c) out of plane bends (wags)
d) torsional modes (changes in the torsional angle)
e) linear bends (for linear molecules)

The internal coordinates are input into the program,

which transforms them to Cartesian coordinates, x. The transformation takes place via

$$R = Bx \qquad 9$$

and the object of BMAT, apart from performing the transformation itself, is to evaluate the B matrix.

UBZM

It is the task of UBZM to generate the potential energy matrix, which describes the possible interactions between the atoms in terms of the force constants. This program uses Urey-Bradley force constants which will be described later; but first it is necessary to consider the most convenient way to express the force constants.

It is simple and logical to define the molecule and its motion in internal coordinate space, but when defining the force constants it is the *only* logical way: if the force constants were defined in space fixed (Cartesian) rather than in molecule fixed (internal) coordinates it would not be possible to transfer the value of the force constants of a particular motion of a particular atom from molecule to molecule, or even from bond to bond within the same molecule. The potential energy

$$2V = \sum_{i=1}^{3N} f_{ij}\, q_i q_j = q^t F_q\, q$$

is therefore redefined in internal coordinate space

$$2V = R^t F_R R \qquad 10$$

As stated earlier the desirable method of doing the calculations is to input a set of force constants which have already been found for molecules similar to the one under investigation, relying on their transferability, and then make small changes until the frequencies calculated fit the observed frequencies. To achieve this F_R is written as

$$F_{ij} = Z_{ijk}\, \delta_k \quad \text{or} \quad F_R = Z\, \delta \qquad 11$$

where δ is a column matrix which consists of the force constants, and the Z matrix determines where in F_R a particular force constant will appear. The Z matrix also contains a weighting factor; it thus has four columns, two for position (i and j), one for the force constant (given by δ_k), and the last one for a weighting factor, which in the case of a general valence force field has the value 1.000 (for an explanation of the weighting factor, see reference 40). For example

1 3 3 1.000

means that row 1 column 3 gets the value of force constants #3, weighted by 1.000. The separation of Z and δ allows us to calculate the Z matrix once only. The force constants are input later in the program NOCO and are easily changed for each run of the program.

It is possible to circumvent the UBZM program and write out the potential energy matrix by hand, using a

general valence force field. However, including all the interaction between the non-bonded atoms for anything but the simplest molecules becomes a mammoth task. It is easier to use a method based on the work of Urey and Bradley (42). They proposed that the interaction between adjacent non-bonded atoms must be similar in kind and magnitude to the forces between inert gas atoms or ions in crystals, that is, similar to Van der Waals forces. Based on their work a method was developed by Simanouti for including these interactions in the vibrational secular equation (43). The Urey-Bradley force constants commonly used in vibrational calculations refer to the definition given by Simanouti. For these programs the Urey-Bradley interactions are defined in the input of UBZM. The interactions are defined for three situations:

i) Interactions between two non-bonded atoms in a tetrahedral arrangement.

ii) Interactions between two atoms which are separated by two bonds and which are not part of a tetrahedral arrangement.

iii) Interactions between two atoms which are separated by three bonds (a cis- or trans-type interaction.)

UBZM calculates the weighting factor (the fourth column of the Z matrix) and outputs the Z matrix (40,41).

NOCO

The input for the program NOCO consists of the force constants, the atomic masses, and the observed frequencies. If there are isotopically substituted species, their atomic masses and observed frequencies are also input. As stated earlier (equation 1) the kinetic energy is given by

$$2T = \Sigma (\dot{q}_i)^2 = \Sigma m_i (\dot{x}_i)^2 = x^t M x$$

where $\cdot$ indicates the time derivative, M is the diagonal matrix of the masses of the atoms 1 to N, and x^t and x are row and column vectors of the $\dot{x}_i$. The advantage of calculating the kinetic energy in mass weighted Cartesian space is that it is already a diagonal matrix. As discussed previously, the potential energy is defined in internal coordinate space:

$$2V = R^t F_R R$$

so that F depends only on the nature of the motion it describes and the atoms to which it refers.

In Schachtschneider's programs Wilson's GF method was used: the kinetic energy was transformed into internal coordinate space, and all the calculations were carried out in internal coordinate space (40). This procedure leads to a nonsymmetric matrix, which has to be diagonalized via a time consuming algorithm. As the programs were adapted for use with a PC it was found that time could be

saved by using a fast algorithm for diagonalizing a symmetric matrix, the Householder diagonalization routine (41). Therefore the secular equation is defined in mass weighted space. The B-matrix is used to transform F_R into Cartesian coordinate space (equation 9):

$$F_x = B^t F_R B \qquad 12$$

and to mass weighted Cartesian space

$$F_q = W B^t F_R B W \qquad 13$$

where $W = M^{-\frac{1}{2}}$, which is already in the diagonal form. This is the quantity we need for the secular equation (equation 6), which is now diagonalized via the Householder diagonalization routine. Solutions to the secular equation gives the energies which are converted to wave numbers. The eigenvector matrix, C, which is obtained in the process, transforms from mass weighted Cartesian to normal coordinate space. This transformation

$$C^t F_q C$$

can be written (equation 12 and 13)

$$C^t W F_x W C$$

from which we define the transformation matrix

$$S = W C \qquad 14$$

which transforms from Cartesian coordinates x to normal coordinates Q; and

$$C^t W B^t F_R B W C$$

from which we get the transformation matrix

$$L = B W C \qquad 15$$

which transforms from internal coordinates to normal coordinates.

Atomic Displacements.

As pointed out earlier we know only the relative amplitudes of the displacements of the atoms during the normal mode (equation 7). The S matrix allows us to find the relative displacement in Cartesian coordinates since

$$x = S\,Q$$

The program is written in such a way that it displays the relative displacements in the x, y, and z direction of each atom during a normal mode.

The Potential Energy Distribution, PED.

The contribution to the potential energy of the force constants to a particular normal mode, i, is given by

$$L_{ji}\, L_{ki}\, F_{jk}$$

where $F_{jk} = \sum_m Z_{jkm}\, \bar{\omega}_m$

The fractional contribution of a particular force constant, $\bar{\omega}_m$, is therefore

$$L_{ji}\, L_{ki}\, Z_{jkm}\, \bar{\omega}_m \,/\, \lambda_i$$

The values for all m's makes up the potential energy distribution, PED, for the i'th normal mode. The program is written in such a way that the PED is displayed for each frequency, together with the force constant number

and description. This is very important: not only do we wish to reproduce the observed frequencies, but we want correspondence between the assignment of the mode and the force constants which contribute to it. For example, if we have assigned a mode to a C-H deformation we want the PED to show that the C-H deformation force constant contributes strongly to that mode.

Summary

The program NOCO outputs the observed frequencies, the calculated frequencies and the difference between the two. It then lists each mode with the description of the observed frequency and the PED's calculated. If there are isotopically substituted species these are calculated and displayed in a similar manner, for a particular set of force constants. There is an option in the program to have this followed by a listing of the atomic displacements in Cartesian coordinates for all normal modes (the S-vector).

It should again be stressed that in carrying out the calculations all factors have to be taken into consideration: frequencies have to match for all isotopically substituted species, and the PED's and displacements have to correspond to the features revealed during the vibrational analysis which was the basis of the calculations. Exactly how this was done in the case of alanyl-alanine

is the subject of the next chapter.

CHAPTER IV

VIBRATIONAL ASSIGNMENT AND NORMAL COORDINATE ANALYSIS OF ALANINE DIPEPTIDE.

Introduction

The overall aim of our research is to obtain conformational information about small peptides, using the technique of vibrational circular dichroism, VCD. Detailed interpretation of VCD requires thorough understanding of the vibrational spectrum of the molecule examined. This study provides an in-depth look at the vibrations of the simplest chiral peptide, L-alanyl-L-alanine.

Historical Sequence of Vibrational Spectroscopy of Peptides.

When vibrational spectroscopists first started examining peptides and proteins they found several vibrations in the infrared which are characteristic of those molecules. Since they all have in common the peptide linkage

it was concluded that the vibrations involved these atoms. The vibrations were named amide I-VII and amide A

and B. It was also found that the frequencies of some vibrations shift as the peptide undergoes conformational changes, and that these frequency shifts can be correlated with secondary structure, such as ß sheets and a helices (44, 45).

Miyazawa et al. carried out an analysis of the model compound N-methylacetamide

to find the normal modes associated with the amide vibrations (46). Our work is mostly concerned with the amide I - III vibrations. The amide I vibration, observed at 1653 cm^{-1}, was assigned by Miyazawa to be mainly due to the C=O stretching vibration. Upon deuteration of the N-H hydrogen the frequency shifts to 1642 cm^{-1}. The amide II vibration is observed at 1567 cm^{-1}, and shifts to 1472 cm^{-1} upon deuteration. They found this band to be largely due to the N-H in plane deformation, with a much smaller contribution from the C-N stretch. They also found that the amide III mode consists of the N-H deformation and, to a lesser extent, of the stretching of the C-N bond. This assignment, however, does not adequately explain the observed sensitivity of the amide III region to conformational changes.

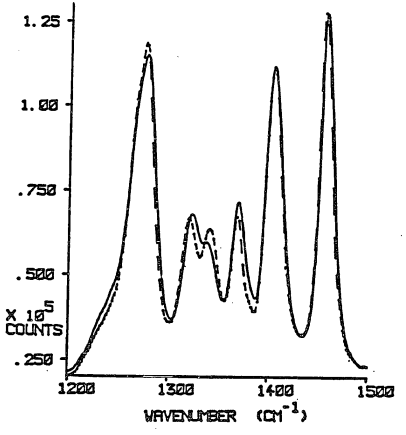

Figure 1. Raman spectra of LL-alanine (solid line) and DL-alanine (broken line) in aqueous solution, concentration app. 0.5 M.

Vibrational Assignment of the Amide III Region.

Our interest in the subject began with the observation that there is a small but clearly reproducible difference between the Raman spectra of aqueous solutions of L-alanyl-L-alanine and D-alanyl-L-alanine (hereafter referred to as LL-alanine and DL-alanine) in the amide III region (Figure 1). This region appears to consist of three bands; the first task was therefore considered to be the thorough understanding of what constitutes these bands in the dipeptide. This was achieved by a careful vibrational analysis based on the Raman studies of LL-alanine and five isotopically substituted species, which revealed that the bands observed in the amide III region are the result of extensive coupling of the N-H deformation with the deformation of the methine groups at both ends of the molecule (29). Since that study is the back ground for the normal coordinate analysis it is here explained in detail.

The original spectra are reproduced in Figure 2. The nomenclature used in that study is adopted here as well. The species

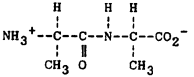

is referred to as CHNHCH,

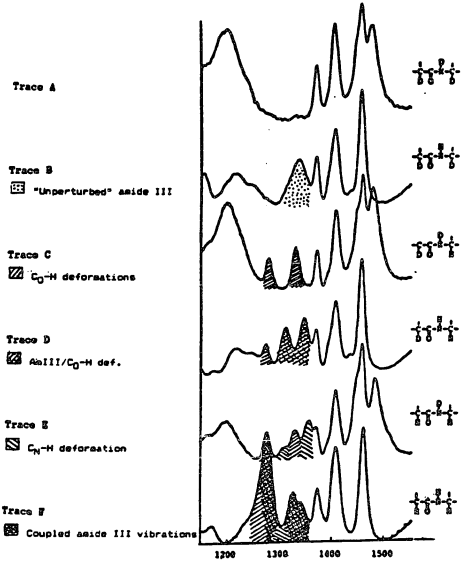

Fig.2 Raman spectra of aqueous solutions of LL-alanine and its isotopically substituted species (29).

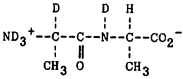

as CDNDCH, and so forth. The six isotopomers studied are: the native molecule, the molecule with one of the methine hydrogens exchanged for deuterium (at the N-terminal) and the molecule with both methine hydrogens exchanged for deuterium. Solutions were made in H_2O and D_2O giving six isotopomers in all, since all labile protons will exchange with deuterium when dissolved in D_2O (all hydrogens at the NH_3^+ and at the peptide linkage). Like alanine the dipeptide exists as a zwitterion in aqueous solution, as indicated in the structures. This is proven by the symmetric and antisymmetric stretch of CO_2^-, which occur at about the same frequencies in the two molecules. The syntheses of these molecules are described in chapter II. The assignments for the vibrations in the amide III region are summarized in Table I (All tables are presented at the end of the chapter to avoid constant interruption of the text).

In alanine, where there is no peptide linkage, there are two strong bands at 1351 and 1301 cm^{-1}, due to the two deformations of the C^*-H (the methine deformation) (28). We shall show that in peptides the amide III vibrations involve the simultaneous motion of the C^*-H and of

the N-H in plane deformation

All conformational sensitivity of the amide III region is believed to be due to this coupled motion. In the following analysis special attention should therefore be paid to presence or absence of methine hydrogens. The methine at the nitrogen end has been named C_N-H and the methine at the carboxylate end has been named C_O-H. As in the case of the C^*-H deformation of alanine mentioned above, there are instances when we have more than one spectral feature due to the same coordinates; in such instances they have been numbered from lower to higher frequencies for easier identification. In the analysis only the amide III region is discussed.

The analysis revealed the following (please refer to Figure 2):

CDNDCD, trace A: In the absence of both methine hydrogens and the N-H hydrogen no vibrations are observed.

CDNHCD, trace B: With only the N-H hydrogen present the only feature is a broad peak centered at 1336 cm^{-1}. This will be referred to as the "unperturbed" amide III mode.

CDNDCH, trace C: Only C_O-H remains undeuterated; the two bands observed are therefore interpreted as being due to

the two deformations of this methine hydrogen, $C_{O}H,1$ and C_{O}-H,2.

CDNHCH, trace D: This might be expected to consist of the "unperturbed" amide III band and the two methine deformations observed in the two previous cases, trace B and C. Instead we see a shift in the positions of the "unperturbed" amide III and the C_{O}-H,2 deformation. This was interpreted as being due to a mixing of the two deformation coordinates, giving rise to two new modes. The C_{O}-H,1 does not shift, and is therefore considered not to take part in this mixing.

CHNDCH, trace E: Four bands are observed: In the absence of the N-H hydrogen the two C_{O}-H deformation reappear at their original, unperturbed positions as seen in trace C. The two other bands are interpreted as being due to the deformations of the C_{N}-H hydrogen. There is no evidence of any coupling of the two methines.

CHNHCH, trace F: This spectrum was interpreted partly on the basis of the above, and partly from a band decomposition. From the previous traces we know that the region contains five distinct coordinates, namely the N-H deformation (the "unperturbed" amide III, trace B) and four C-H deformations (trace E). Thus, whether or not there is any mixing of the coordinates we should observe five bands. Trace F shows only three clearly observable bands;

therefore, a band decomposition was carried out. The band decomposition showed the possible frequencies of the bands and this, together with the information gained from the previous spectra, allowed the spectrum to be interpreted as follows: the two lower frequency deformations of the methines at the C- and N-terminal respectively (C_OH,1 and C_NH,1) remain unperturbed; the remaining three bands are due to the mixing of the amide III and the remaining two methine deformation modes to form three new modes which are a combination of the original unperturbed modes (amIII,1 ; amIII,2 ; and amIII,3). This interpretation was later supported by vibrational circular dichroism studies which will be discussed in chapter VI (47).

Normal Coordinate Calculations.

The purpose of the normal coordinate calculations presented in the following sections was to derive a force field which agrees with all the vibrational features of alanyl-alanine discussed above. This entailed reproducing the observed spectra and the mixing of the coordinates, which would hopefully lead to a better understanding of the nature of the mixed modes.

For the calculations the molecule was defined as shown in Figure 3. It was simplified by treating the methyl groups and the NH_3^+ group as point masses. The bond lengths, bond angles, and atomic weights used are

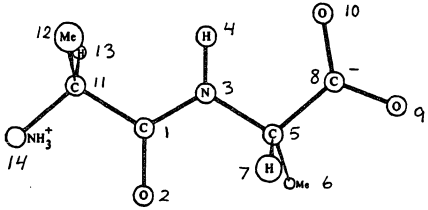

Figure 3. LL-alanine as defined in the normal coordinate calculation. CH_3 and NH_3^+ are treated as point masses.

summarized in Table II. As discussed in Chapter III the calculations were carried out using programs adapted from Schachtschneider, with a Urey-Bradley force field (40, 41). In the definition of the Urey-Bradley force field only gem and tetra interactions were considered, mainly in order to keep the number of force constants manageable. The normal coordinate calculations were carried out for all six isotopically substituted species, with a final number of forty seven force constants.

Requirements of the Urey-Bradley Force Field.

With so many variables it is not surprising that there is more than one force field which could reproduce the observed frequencies within a few percent error. In selecting the one which is presented here, certain criteria were established:

1) The force constants should be close to the ones already reported for alanine whenever appropriate (28).

2) There should be agreement between the observed and calculated frequencies in the amide III region.

3) There should be agreement between the calculated motions of the molecule and interpretation of the observed spectra.

4) The calculations should reproduce the frequencies observed in the amide III region, as well as the frequencies above and immediately below that region.

The following is a discussion of how the criteria were met:

1) Whenever possible, comparison was made to the values obtained by Diem (28) because his results were based on similar calculations, involving five isotopically substituted species of alanine. The usefulness of that study is shown by the close agreement between the two sets of force constants. The results by Gupta et al. (48), although also useful, were in some cases quite different. As stressed in Chapter III (in the section "Spectroscopy and Normal Coordinate Calculations") it is necessary to have accurate vibrational assignments, based on IR and/or Raman studies of several isotopically substituted species, to get a reliable force field. Gupta's study was based only on solid state infrared spectra of undeuterated alanyl-alanine, and many of the reported frequencies were only calculated and not observed; it is therefore not surprising that the agreement between his and our force constants is poor in some cases.

2) The ideal was that the difference between observed and calculated frequencies should be less than one percent. However, since some force constants were omitted, namely those for the cis interactions and for the torsional modes, the force field had some limitations. Therefore obtaining a perfect or near perfect fit was considered

less important than fulfilling requirement 3, discussed next.

3) The vibrational analysis had shown that in the spectrum of CDNDCH (Figure 2, trace C) there are two C_O-H deformation modes, similar to the unperturbed modes observed in alanine. In the spectrum of CHNDCH (Figure 2, trace E) there are two C_O-H and two C_N-H deformation modes, which appear to be uncoupled. It was required that the displacement vectors resulting from the calculations should show this unmixed behavior of the four modes in CHNDCH.

4) This requirement turned out to be the most troublesome: it was straight forward, if time consuming, to fit the frequencies above the amide III region, but impossible to fit the ones below that region. The higher frequencies had been assigned in the vibrational analysis and it remained only to identify the calculated frequencies, and make adjustments to the force constants for a good fit. In the region below the amide III, which is commonly referred to as the skeletal stretching region, no assignments had been made. Since this region had been thoroughly analyzed for alanine (28) and since the original LL-alanine Raman spectra were still available, an analysis was attempted. The attempt failed completely: The modes due to the deformations of the deuterated species mix with or overlap the skeletal stretches in

unpredictable ways. In alanine Diem et al. assigned the frequencies of the skeletal stretches involving the C*-C(methyl), C*-C(carboxylic) and C-N moieties (28). In the dipeptide, however, with two amino acids, it was impossible to discern to which amino acid a C-C or C-N stretch belonged; it would require a new set of isotopic substitutions of the nitrogen or carbon atoms to sort out the region. As it turned out it did not matter for our calculations of the amide III region, for it soon became obvious that adjustments to the force constants belonging to the skeletal stretches have little or no effect on the frequencies calculated for the amide III region. Therefore the attempted analysis was abandoned together with the attempt to fit the frequencies below the amide III region.

Results and Discussion.

The criteria for choosing the force constants have already been discussed, and the final values are presented in Table III. They are compared to the values which formed the starting point in the calculation.

The calculated frequencies are tabulated in Table IV together with the observed frequencies for all six species from 3500 - 1200 cm^{-1}. This is done to show the extent of the error for the whole region. Since our main

interest was the amide III region it did not matter so much if one of the higher frequencies were off by a few percent. This view is justified, just as in the case of the frequencies below the amide III region, by the observation that minor changes to the force constants of those modes have little or no influence on the frequencies in the region of interest. The assignments were verified by inspection of the potential energy distribution (PED) and the Cartesian displacement vector belonging to each mode. (The displacement vectors will hereafter be referred to as the s-vectors.)

In the following only the results from the amide III region will be discussed. In Table V the observed and calculated frequencies have been repeated, together with the PED's. Only those force constants which contributed more than 10% have been included in the PED's. Also included are references to the table containing the s-vector for the frequency reported.

It is easiest to understand the different modes by looking at the s-vectors. Therefore the spectra will be analyzed with specific reference to the s-vectors, which have been reproduced in Tables VI to XX. In these tables the displacements have also been depicted graphically. The numbers of the atoms are the same as those that were defined in the normal coordinate analysis (cf. Figure 3).

CDNDCD (Figure 2, trace A): Since all the hydrogens which

are involved in the deformations in the amide III region have been exchanged for deuterium there are no vibrations in this region, just as expected. This dipeptide will therefore not be discussed further.

CDNHCD (Figure 2, trace B): The s-vector, Table VI, shows that the "unperturbed" amide III consists mostly of the N-H in plane deformations and, to a lesser extent, of the C-N stretch. Interestingly enough this is in accord with the findings of Miyazawa (46): with both methine hydrogens exchanged for deuterium the surroundings of the peptide linkage is almost identical to that of the N-methylacetamide.

CDNHCD

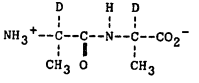

N-methylacetamide

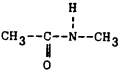

It is therefore appropriate that this should be called the "unperturbed" amide III vibration.

CDNDCH (Figure 2, trace C) The calculations are in complete agreement with the vibrational analysis: Table VII

and VIII show that the two vibrations observed are the C_O-H,2 and C_O-H,1 deformations, respectively. They are at approximately ninety degrees to each other as one would expect.

CDNHCH (Figure 2, trace D): There are three modes: Table IX and X show that the two higher frequency modes consist of a mixing of the coordinates of the "unperturbed" amide III and the C_O-H,2 deformation. In one of these, (Am3/CH),1, all the deformations are in the xy plane. The remaining mode, Table XI, was called C_O-H,1 in the vibrational analysis, but in the calculations there seems to be quite a lot of contribution to this mode from the N-H in plane deformation. The reason for retaining the name is that it corresponds to the spectral analysis. It is possible that it would be more correct to consider all three modes to be mixed modes; however, it is clearly evident from the spectra that the two higher frequency modes are coupled (the intensities changes and they move apart) whereas the low frequency mode does not appear to shift. That does not necessarily mean that the mode is completely unaffected by the presence of the N-H hydrogen: it could mean that the effect is too small to be clearly seen in the spectrum. The main point is that we do observe a mixing of the coordinates in the two higher frequency modes, which is in agreement with the spectral analysis.

CHNDCH (Figure 2,trace E): The spectral analysis shows four separate methine deformation modes, and this is confirmed by the calculations. Table XII and XIV show clearly the deformation modes of the C_N-H hydrogen. They occur at approximately ninety degrees to each other. Table XIII and XV show the deformation modes of the C_O-H hydrogen, and these modes, too, are at approximately ninety degrees to each other. Comparison between Table XIII (CHNDCH, C_O-H,2) and Table VII (CDNDCH, C_O-H,2) reveal that these are very similar, especially if we disregard the tetrahedral arrangement at the N-terminal. Comparison between Table XV (C_O-H,1) and Table VIII (CDNDCH, C_O-H,1) are also very similar (although the motions are not in phase). This is exactly what we would expect of the two molecules, which both have unperturbed C_O-H deformations (in the absence of the N-H deformation).

CHNHCH (Figure 2, trace F): There are five modes to consider in this molecule. Inspection of the s-vectors reveals that the mode calculated to occur at 1284.0 cm^{-1} is the C_N-H deformation mode, which is observed at 1302 cm^{-1}: The s-vector of this mode, Table XIX, is virtually identical to the s-vector of the C_N-H,1 deformation in CHNDCH, Table XIV, (they are out of phase). Similarly, the identity of the lowest frequency mode, Table XX, can

be established by comparison to table XI (CDNHCH, C_O-H). Although they are not identical (and out of phase), they are sufficiently similar to leave no doubt that they represent the same mode, namely C_O-H,1.

This leaves the three "true" amide III vibrations. All three have contributions from the two remaining methine deformations (C_O-H,2 and C_N-H,2). AmIII,3, Table XVI, also has a large contribution from the N-H in-plane deformation, whereas amIII,2, Table XVII, has only a small contribution from this deformation. AmIII,1, Table XVIII, is the most delocalized mode: it has contributions from the N-H in plane deformation and the C-N stretch (atoms 1 and 3) in addition to the two methine deformations. It thus represents the most highly mixed of all the modes described so far. That the s-vector is close to the true description is supported by the fact that this mode always disappears completely upon deuteration: in the absence of any one of the contributing coordinates it vanishes.

Conclusion.

Using a force field which is very similar to the one developed for alanine it has been shown that it is possible to reproduce the vibrational frequencies for LL-alanine and its isotopomers in the region from 3500 to 1200 cm^{-1}. In particular we have succeeded in analyzing

the amide III region in a manner which is consistent with the observed spectra. The calculations have further supported the view that this region consists of a complex coupling of the N-H hydrogen deformation with the deformations of the two adjacent methines and that the region changes drastically if any of the three components is not present. Since the force field was defined without any terms for the cis interaction, i.e., without any term for through-space interaction of atoms three bonds apart, it appears that it is not necessary to invoke a through space interaction such as a coupled oscillator mechanism to account for the observed mixing. This is particularly important since the C-H bond has little polarity, making it impossible to account for the observed coupling via a coupled oscillator mechanism. The coupling observed must therefore be a potential or kinetic energy coupling.

Table I

	C_OH,1 def	Am3,1	C_NH,1 def	Am3,2	(Am3/C_OH),1
CDNHCD					
CDNDCH	1279				
CDNHCH	1274				1311
CHNDCH	1276		1305		
CHNHCH	1266*	1281*	1302*	1325*	

	"unperturbed"			
	C_OH, 2 def	Am3	Am3,3	(Am3/C_OH),2	C_NH,2 def
CDNHCD		1336			
CDNDCH	1330				
CDNHCH				1346	
CHNDCH	1329				1355
CHNHCH			1345*		

Vibrational frequencies in the amide III region from Raman data (29). CDNDCD has not been included as it has no vibrations in this region. The frequencies marked with an asterisk were found via a band decomposition.

Table II

C-H	1.070	
C-C	1.516	
C-(CH_3)	1.53	
C-N	1.472	
C-(NH_3^+)	1.479	
C..N	1.322	(peptide linkage)
C..O	1.23	(peptide linkage)
C..O	1.26	(carboxylate)
N-H	1.038	

C	12.01
H	1.008
D	2.016
N	14.007
O	15.998

The top shows the bond lengths in Ångströms. .. indicates partial double bond.
The bottom shows the atomic masses. The point masses were the sum of the masses of the constituent atoms.

Table III

No.	Final value	Initial value	Definition
1	8.40	8.40*	C_c=O str (peptide linkage)
2	6.500	6.35*	C_c-N str (" ")
3	5.100	4.778	N-H str
4	2.400	2.500	N-C^* str
5	1.800	1.800	C^*-m str
6	4.150	4.101	C^*-H str
7	2.400	3.010	C^*-C_c str
8	7.450	7.355	C_c=O str
9	2.700	2.500	C^*-a str
10	0.450	0.75*	O-C_c-N bend (peptide linkage)
11	0.300	0.219	O-C_c-C^* bend
12	0.500	0.500	C_c-C^*-m bend
13	0.430	0.398	C_c-C^*-H bend
14	0.720	0.720	C^*-C_c-N bend
15	0.360	0.368	m-C^*-H bend
16	0.370	0.353	H-C^*-a bend
17	0.720	0.720	m-C^*-a bend
18	0.400	0.418	H-N-C^* bend
19	0.720	0.720	N-C^*-m bend
20	0.353	0.353	N-C^*-H bend
21	0.500	0.500	N-C^*-C_o bend

22	0.219	0.219	C^*-C_o-O bend
23	0.500	0.42*	C_c=O wag
24	0.185	0.09*	N-H wag
25	0.429	0.529	C_o-O wag
26	0.400	0.40*	C_c-N-C^* bend
27	0.130	0.130	O-C_o-O bend
28	0.479	0.264	C_c..C^*..m tet
29	0.778	0.580	C_c..C^*..H tet
30	0.545	0.387	C_c..C^*..a tet
31	0.387	0.490	m..C^*..H tet
32	0.300	0.778	m..C^*..a tet
33	0.580	0.499	H..C^*..a tet
34	0.053	0.053	rho
35	1.000	1.075	C^*..C_c..O gem
36	0.700	0.700	C^*..C_c..N gem
37	1.400	2.50	N..C_c..O gem (peptide linkage)
38	0.550	0.619	H..N..C_c gem (peptide linkage)
39	0.550	0.50*	C^*..N..C_c gem
40	0.878	0.778	N..C^*..m tet
41	0.499	0.499	N..C^*..H tet
42	0.387	0.387	n..C^*..C_o tet
43	0.500	0.264	m..C^*..C_o tet
44	0.480	0.580	H..C^*..C_o tet
45	1.000	1.075	O..C_o..C^* gem

46	3.100	3.184	O..C_o..O gem
47	1.850	1.800	C^*-C_c str

Urey-Bradley force constants used in the normal coordinate calculations of LL-alanine. The units are mdyn/Å for the stretching and non-bonded interaction constants; the bending, wagging and the intermolecular tension (rho) constants are in mdyn/radian. C_c refers to the carbonyl carbon, C_o to the carboxylate carbon, and C^* to a chiral carbon. "m" refers to a methyl point group and "a" refers to the NH_3^+ point group. Initial values marked * refer to Gupta et al. (48). All other initial values are from reference 28.

Table IV

	CDNDCD		CDNHCD		CDNDCH	
	obs.	calc.	obs.	calc.	obs.	calc.
Amide A	2265.0	2351.6	3215.0	3220.7	2265.0	2351.2
C_N-H str.	2210.0	2176.4	2210.0	2176.4	2210.0	2176.4
C_O-H str.	2210.0	2169.0	2210.0	2169.5	2970.0	2970.4
Amide I	1663.0	1678.4	1680.0	1682.4	1664.0	1678.4
CO_2^- as	1584.0	1585.8	1584.0	1591.1	1590.0	1588.3
Amide II	1478.4	1450.3	1570.0	1576.0	1479.0	1451.0
CO_2^- ss	1406.0	1410.7	1406.0	1411.1	1408.0	1412.4
Amide III	-	-	1336.0	1314.9	-	-
" "	-	-	-	-	-	-
" "	-	-	-	-	-	-
C_N-H def.	-	-	-	-	-	-
" "	-	-	-	-	-	-
C_O-H def.	-	-	-	-	1330.0	1329.8
" "	-	-	-	-	1279.0	1278.4

CDNHCH		CHNDCH		CHNHCH	
obs.	calc.	obs.	calc.	obs.	calc.
3215.0	3220.9	2265.0	2351.2	3215.0	3220.9
2210.0	2176.4	2970.0	2983.2	2970.0	2983.2
2970.0	2970.1	2970.0	2970.4	2970.0	2970.1
1680.0	1682.5	1665.0	1681.5	1680.0	1685.6
1584.0	1592.5	1592.0	1588.3	1584.0	1592.7
1570.0	1578.1	1483.0	1455.4	1570.0	1578.4
1407.0	1412.9	1407.0	1412.4	1407.0	1413.0
1346.0	1333.5	-	-	1345.0*	1355.1
1311.0	1312.2	-	-	1325.0*	1330.7
-	-	-	-	1281.0*	1307.8
-	-	1355.0	1343.2	-	-
-	-	1305.0	1284.0	1302.0*	1284.0
-	-	1329.0	1329.7	-	-
1274.0	1273.8	1276.0	1278.3	1266.0*	1273.3

Observed and calculated frequencies in cm^{-1}, from 3500 to 1200 cm^{-1} for all six species. The frequencies marked * were found via a band decomposition.

Table V

obs.	calc.	PED's (%)	s-vector
CDNDCD			
There are no vibrations in this region.			
CDNHCD			
1336.0	1314.9	1(17),2(28),18(13),38(16) "unperturbed" amIII	Table VI
CDNDCH			
1330.0	1329.8	13(37),15(14),30(10),44(19)	C_O-H def Table VII
1279.0	1278.4	15(21),20(32),30(18),41(22)	" " Table VIII
CDNHCH			
1346.0	1333.5	13(25),15(13),44(13)	Am3/CH def Table IX
1311.0	1312.2	1(12),2(16),13(13),38(12)	" " Table X
1274.0	1273.8	15(22),20(26),30(18),41(19)	C_O-H,1 def Table XI
CHNDCH			
1355.0	1343.2	13(38),15(11),33(24)	C_N-H,2 def Table XII
1329.0	1329.7	13(36),15(14),30(10),44(19)	C_O-H,2 def Table XIII
1305.0	1284.0	15(24),16(31),28(21),33(20)	C_N-H,1 def Table XIV

1276.0	1278.3	15(21),20(31),30(18),41(22)	C_O-H,1 def
			Table XV
CHNHCH			
1345.0	1355.1	13(31),33(25)	AmIII,3
			Table XVI
1325.0	1330.7	13(33),15(14),30(10),44(15)	AmIII,2
			Table XVII
1302.0	1284.0	15(24),16(31),28(21),30(20)	C_N-H,1 def
			Table XIX
1281.0	1307.8	1(14),2(14),13(13),38(11)	AmIII,1
			Table XVIII
1266.0	1273.3	15(22),20(25),30(18),41(18)	C_O-H,1 df
			Table XX

Observed and calculated frequencies for the amide III region with corresponding PED's and s-vectors.

Table VI. L-Ala-d_1-L-Ala-d_1 in H_2O, CDNHCD

	DEL X	DEL Y	DEL Z
ATOM # 1,C_c	.0562	.1745	.0034
ATOM # 2,O	-.0869	-.0085	-.0003
ATOM # 3,N	.0367	-.0789	-.0003
ATOM # 4,H	.0366	-.5632	-.0003
ATOM # 5,C*	.0425	.0040	-.0073
ATOM # 6,CH_3	-.0028	-.0005	.0003
ATOM # 7,H	-.0077	.0025	.0346
ATOM # 8,C_α	.0042	-.0077	.0024
ATOM # 9,O	.0069	.0138	-.0005
ATOM # 10,O	-.0152	-.0027	-.0005
ATOM # 11,C*	-.0130	-.0276	-.0055
ATOM # 12,CH_3	-.0015	.0000	.0009
ATOM # 13,H	-.0081	-.0238	.0132
ATOM # 14,NH_3^+	-.0007	-.0022	-.0004

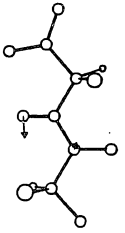

"Unperturbed" Amide III, obs. freq. 1336 cm^{-1}.

calc. freq. 1314.9 cm^{-1}.

Table VII. L-Ala-d_1-L-Ala in D_2O, CDNDCH

	DEL X	DEL Y	DEL Z
ATOM # 1,C_c	-.0042	-.0396	-.0005
ATOM # 2,O	.0050	.0028	.0001
ATOM # 3,N	.0049	.0113	.0037
ATOM # 4,H	.0093	.0227	.0019
ATOM # 5,C*	-.0748	.0906	.0437
ATOM # 6,CH_3	.0095	-.0011	.0127
ATOM # 7,H	.5194	-.5857	-.3217
ATOM # 8,C_o	.0340	-.0080	-.0552
ATOM # 9,O	-.0003	-.0095	.0067
ATOM # 10,O	-.0205	-.0068	.0067
ATOM # 11,C*	.0024	.0079	.0009
ATOM # 12,CH_3	.0002	-.0002	-.0002
ATOM # 13,H	.0008	.0016	-.0018
ATOM # 14,NH_3^+	.0004	.0004	.0001

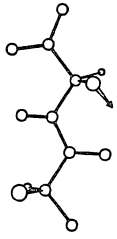

C_o-H,2 def. obs. freq. 1330 cm^{-1}.

calc. freq. 1329.8 cm^{-1}.

Table VIII. L-Ala-d_1-L-Ala in D_2O, CDNDCH

	DEL X	DEL Y	DEL Z
ATOM # 1,C_c	.0011	-.0126	-.0051
ATOM # 2,O	-.0038	.0015	.0009
ATOM # 3,N	.0073	-.0023	.0288
ATOM # 4,H	.0217	-.0355	-.0097
ATOM # 5,C*	.0531	.0853	-.0346
ATOM # 6,CH_3	-.0126	-.0027	-.0208
ATOM # 7,H	-.5171	-.6251	.4101
ATOM # 8,C_o	.0068	.0003	-.0007
ATOM # 9,O	-.0007	-.0119	-.0010
ATOM # 10,O	-.0069	.0013	-.0010
ATOM # 11,C*	.0003	.0038	.0018
ATOM # 12,CH_3	.0001	-.0002	-.0002
ATOM # 13,H	.0020	.0010	-.0001
ATOM # 14,NH_3^+	.0003	.0000	.0000

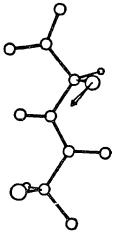

C_o-H,1 def. obs. freq. 1279 cm^{-1}.

calc. freq. 1278.4 cm^{-1}.

Table IX. L-Ala-d_1-L-Ala in H_2O, CDNHCH

		DEL X	DEL Y	DEL Z
ATOM #	1,C_c	-.0289	-.1063	-.0016
ATOM #	2,O	.0411	.0058	.0002
ATOM #	3,N	-.0113	.0494	.0014
ATOM #	4,H	-.0101	.2271	.0046
ATOM #	5,C*	-.0815	.0657	.0400
ATOM #	6,CH_3	.0095	-.0005	.0125
ATOM #	7,H	.4824	-.4500	-.3146
ATOM #	8,C_o	.0265	-.0029	-.0465
ATOM #	9,O	-.0028	-.0123	.0057
ATOM #	10,O	-.0118	-.0049	.0057
ATOM #	11,C*	.0079	.0165	.0030
ATOM #	12,CH_3	.0008	-.0001	-.0005
ATOM #	13,H	.0038	.0122	-.0070
ATOM #	14,NH_3^+	.0004	.0014	.0002

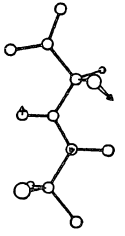

AmIII/CH,2 def. obs. freq. 1346 cm^{-1}.

calc. freq. 1333.5 cm^{-1}.

Table X. L-Ala-d_1-L-Ala in H_2O, CDNHCH

	DEL X	DEL Y	DEL Z
ATOM # 1,C_c	.0462	.1238	.0014
ATOM # 2,O	-.0736	-.0052	.0000
ATOM # 3,N	.0383	-.0608	.0096
ATOM # 4,H	.0424	-.4867	-.0029
ATOM # 5,C*	.0093	.0786	.0120
ATOM # 6,CH_3	-.0004	-.0020	.0012
ATOM # 7,H	.1241	-.5079	-.0278
ATOM # 8,C_o	.0223	-.0095	-.0312
ATOM # 9,O	.0048	.0014	.0035
ATOM # 10,O	-.0239	-.0052	.0035
ATOM # 11,C*	-.0095	-.0184	-.0038
ATOM # 12,CH_3	-.0011	-.0001	.0006
ATOM # 13,H	-.0061	-.0193	.0104
ATOM # 14,NH_3^+	-.0003	-.0016	-.0003

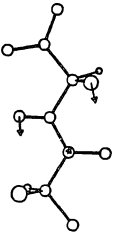

AmIII/CH,1 def. obs. freq. 1311 cm^{-1}.

calc. freq. 1312.2 cm^{-1}.

Table XI. L-Ala-d_1-L-Ala in H_2O, CDNHCH

		DEL X	DEL Y	DEL Z
ATOM #	1,C_c	.0150	.0684	.0064
ATOM #	2,O	-.0250	-.0044	-.0010
ATOM #	3,N	.0046	-.0148	-.0278
ATOM #	4,H	-.0053	-.1967	.0218
ATOM #	5,C*	-.0408	-.0730	.0370
ATOM #	6,CH_3	.0120	.0024	.0219
ATOM #	7,H	.5529	.5238	-.4159
ATOM #	8,C_o	-.0029	-.0016	-.0067
ATOM #	9,O	.0029	.0145	.0019
ATOM #	10,O	-.0010	-.0030	.0019
ATOM #	11,C*	-.0039	-.0152	-.0036
ATOM #	12,CH_3	-.0006	.0004	.0005
ATOM #	13,H	-.0050	-.0073	.0046
ATOM #	14,NH_3^+	-.0008	-.0004	-.0001

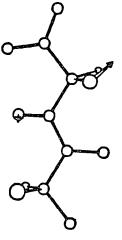

C_OH,1 def. obs. freq. 1274 cm^{-1}.

calc. freq. 1273.8 cm^{-1}.

Table XII. L-Ala-L-Ala in D_2O, CHNDCH

	DEL X	DEL Y	DEL Z
ATOM # 1,C_c	-.0328	-.0190	.0441
ATOM # 2,O	.0325	-.0014	-.0031
ATOM # 3,N	-.0007	.0225	-.0058
ATOM # 4,H	-.0032	-.0528	.0040
ATOM # 5,C^*	.0092	-.0168	-.0047
ATOM # 6,CH_3	-.0016	-.0001	-.0006
ATOM # 7,H	-.0543	.0758	.0347
ATOM # 8,C_o	-.0045	.0022	.0062
ATOM # 9,O	-.0003	.0007	-.0007
ATOM # 10,O	.0025	.0008	-.0007
ATOM # 11,C^*	.0388	.0813	-.0374
ATOM # 12,CH_3	-.0083	-.0020	-.0124
ATOM # 13,H	-.3707	-.7463	.3058
ATOM # 14,NH_3^+	-.0052	-.0045	-.0059

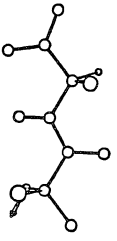

C_N-H,2 def. obs. freq. 1355 cm^{-1}.

calc. freq. 1343.2 cm^{-1}.

Table XIII. L-Ala-L-Ala in D_2O, CHNDCH

	DEL X	DEL Y	DEL Z
ATOM # 1,C_c	-.0073	-.0415	.0042
ATOM # 2,O	.0082	.0027	-.0002
ATOM # 3,N	.0049	.0132	.0031
ATOM # 4,H	.0091	.0180	.0023
ATOM # 5,C^*	-.0743	.0894	.0435
ATOM # 6,CH_3	.0094	-.0011	.0127
ATOM # 7,H	.5167	-.5807	-.3200
ATOM # 8,C_o	.0337	-.0078	-.0548
ATOM # 9,O	-.0003	-.0094	.0066
ATOM # 10,O	-.0204	-.0067	.0066
ATOM # 11,C^*	.0059	.0169	-.0029
ATOM # 12,CH_3	-.0006	-.0004	-.0013
ATOM # 13,H	-.0314	-.0781	.0258
ATOM # 14,NH_3^+	-.0002	-.0002	-.0007

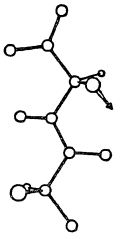

C_O-H,2 def. obs. freq. 1329 cm^{-1}.

calc. freq. 1329.7 cm^{-1}.

Table XIV. L-Ala-L-Ala in D_2O, CHNDCH

	DEL X	DEL Y	DEL Z
ATOM # 1,C_c	.0082	.0094	-.0004
ATOM # 2,O	-.0154	-.0031	-.0007
ATOM # 3,N	.0030	.0066	-.0033
ATOM # 4,H	.0027	.0006	.0010
ATOM # 5,C*	-.0072	-.0103	.0040
ATOM # 6,CH_3	.0011	.0002	.0024
ATOM # 7,H	.0588	.0449	-.0449
ATOM # 8,C_o	-.0002	-.0001	-.0012
ATOM # 9,O	.0002	.0016	.0003
ATOM # 10,O	.0000	-.0004	.0003
ATOM # 11,C*	.0711	-.0594	-.0350
ATOM # 12,CH_3	-.0138	-.0001	-.0217
ATOM # 13,H	-.6511	.4771	.4347
ATOM # 14,NH_3^+	.0071	.0080	.0197

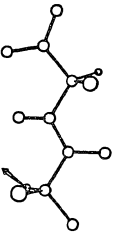

C_N-H,1 def. obs. freq. 1305 cm^{-1}.

calc. freq. 1284.0 cm^{-1}.

Table XV. L-Ala-L-Ala in D_2O, CHNDCH

	DEL X	DEL Y	DEL Z
ATOM # 1,C_c	-.0016	.0119	.0044
ATOM # 2,O	.0051	-.0011	-.0008
ATOM # 3,N	-.0077	.0015	-.0285
ATOM # 4,H	-.0221	.0362	.0096
ATOM # 5,C^*	-.0526	-.0847	.0343
ATOM # 6,CH_3	.0126	.0027	.0206
ATOM # 7,H	.5137	.6238	-.4076
ATOM # 8,C_o	-.0068	-.0003	.0008
ATOM # 9,O	.0007	.0118	.0010
ATOM # 10,O	.0070	-.0013	.0010
ATOM # 11,C^*	-.0085	.0008	.0024
ATOM # 12,CH_3	.0015	.0003	.0026
ATOM # 13,H	.0698	-.0380	-.0485
ATOM # 14,NH_3^+	-.0009	-.0007	-.0019

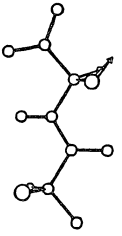

C_O-H,1 def. obs. freq. 1276 cm^{-1}.

calc. freq. 1278.3 cm^{-1}.

Table XVI. L-Ala-L-Ala in H_2O, CHNHCH

		DEL X	DEL Y	DEL Z
ATOM #	1,C_c	-.0047	-.0802	-.0407
ATOM #	2,O	.0184	.0055	.0028
ATOM #	3,N	-.0198	.0385	.0042
ATOM #	4,H	-.0189	.2806	-.0068
ATOM #	5,C^*	-.0299	.0055	.0084
ATOM #	6,CH_3	.0031	.0005	.0030
ATOM #	7,H	.1111	-.0587	-.0851
ATOM #	8,C_o	.0013	.0050	-.0081
ATOM #	9,O	-.0034	-.0081	.0010
ATOM #	10,O	.0044	.0003	.0010
ATOM #	11,C^*	-.0256	-.0601	.0351
ATOM #	12,CH_3	.0079	.0018	.0104
ATOM #	13,H	.3307	.6998	-.2781
ATOM #	14,NH_3^+	.0049	.0054	.0058

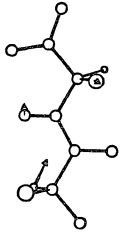

AmIII,3 obs. freq. 1345 cm^{-1},
calc. freq. 1355.1 cm^{-1}.

Table XVII. L-Ala-L-Ala in H_2O, CHNHCH

	DEL X	DEL Y	DEL Z
ATOM # 1,C_c	-.0226	-.0690	.0135
ATOM # 2,O	.0275	.0034	-.0009
ATOM # 3,N	-.0006	.0309	.0008
ATOM # 4,H	.0009	.0828	.0073
ATOM # 5C*	-.0745	.0760	.0409
ATOM # 6,CH_3	.0090	-.0009	.0124
ATOM # 7,H	.4882	-.5090	-.3081
ATOM # 8,C_o	.0298	-.0056	-.0499
ATOM # 9,O	-.0013	-.0101	.0061
ATOM # 10,O	-.0165	-.0058	.0061
ATOM # 11,C*	.0165	.0377	-.0106
ATOM # 12,CH^3	-.0022	-.0008	-.0041
ATOM # 13,H	-.1119	-.2303	.0908
ATOM # 14,NH_3^+	-.0012	-.0008	-.0018

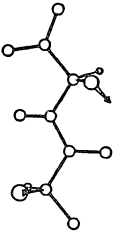

AmIII,2 obs. freq. 1325 cm^{-1}.

calc. freq. 1330.7 cm^{-1}.

Table XVIII. L-Ala-L-Ala in H_2O, CHNHCH

	DEL X	DEL Y	DEL Z
ATOM # 1,C_c	.0517	.1228	-.0153
ATOM # 2,O	-.0778	-.0045	.0013
ATOM # 3,N	.0351	-.0595	.0125
ATOM # 4,H	.0397	-.4519	-.0081
ATOM # 5,C*	.0191	.0698	.0048
ATOM # 6,CH_3	-.0019	-.0018	-.0012
ATOM # 7,H	.0387	-.4568	.0268
ATOM # 8,C_o	.0179	-.0078	-.0240
ATOM # 9,O	.0045	.0015	.0026
ATOM # 10,O	-.0209	-.0042	.0026
ATOM # 11,C*	-.0232	-.0483	.0113
ATOM # 12,CH_3	.0022	.0008	.0050
ATOM # 13,H	.1271	.2281	-.0988
ATOM # 14,NH_3^+	.0011	.0005	.0015

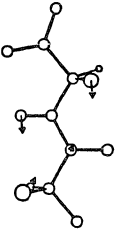

AmIII,1 obs. freq. 1281 cm^{-1}.

calc. freq. 1307.8 cm^{-1}.

Table XIX. L-Ala-L-Ala in H_2O, CHNHCH

	DEL X	DEL Y	DEL Z
ATOM # 1,C_c	-.0083	-.0095	.0004
ATOM # 2,O	.0156	.0031	.0007
ATOM # 3,N	-.0035	-.0066	.0031
ATOM # 4,H	-.0027	.0008	-.0021
ATOM # 5,C^*	.0068	.0097	-.0037
ATOM # 6,CH_3	-.0010	-.0002	-.0023
ATOM # 7,H	-.0548	-.0400	.0417
ATOM # 8,C_o	.0002	.0001	.0012
ATOM # 9,O	-.0002	-.0015	-.0002
ATOM # 10,O	.0001	.0004	-.0002
ATOM # 11,C^*	-.0711	.0595	.0350
ATOM # 12,CH_3	.0138	.0001	.0217
ATOM # 13,H	.6513	-.4776	-.4349
ATOM # 14,NH_3^+	-.0071	-.0080	-.0197

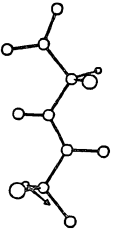

C_N-H,1 def., obs. freq. 1302 cm^{-1} .

calc. freq. 1284.0 cm^{-1}.

This displacement vector is almost identical to C_N-H,1 in L-Ala-L-Ala in D_2O

Table XX. L-Ala-L-Ala in H_2O, CHNHCH

		DEL X	DEL Y	DEL Z
ATOM #	1,C_c	-.0169	-.0716	-.0022
ATOM #	2,O	.0268	.0041	.0006
ATOM #	3,N	-.0048	.0169	.0267
ATOM #	4,H	.0048	.2072	-.0204
ATOM #	5,C^*	.0391	.0710	-.0365
ATOM #	6,CH_3	-.0118	-.0024	-.0217
ATOM #	7,H	-.5466	-.5120	.4101
ATOM #	8,C_o	.0027	.0016	.0069
ATOM #	9,O	-.0030	-.0144	-.0019
ATOM #	10,O	.0015	.0030	-.0019
ATOM #	11,C^*	.0155	.0173	-.0042
ATOM #	12,CH_3	-.0018	-.0006	-.0039
ATOM #	13,H	-.0973	.0005	.0683
ATOM #	14,NH_3^+	.0013	.0007	.0018

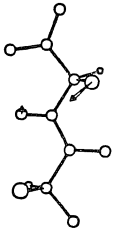

C_O-H,1 def., obs. freq. 1266 cm^{-1}.

calc. freq. 1273.3 cm^{-1}.

CHAPTER V

THE THEORY OF VIBRATIONAL OPTICAL ACTIVITY.

The Dipole Strength and the Rotatory Strength of a Transition.

The quantity measured in the vibrational circular dichroism experiment is the differential absorption of left and right circularly polarized light. This is usually expressed in terms of Kuhn's dissymmetry factor, g (50):

$$g = \frac{E_L - E_R}{\frac{1}{2}(E_L + E_R)}$$

where E_L and E_R are the absorption coefficients for left and right circularly polarized light respectively. The aim of this chapter is to show how this experimentally measured quantity is related to the properties of the molecule under investigation.

It is possible via quantum mechanical considerations to come to the following relationship:

$$g = \frac{E_L - E_R}{\frac{1}{2}(E_L + E_R)} = \frac{4R}{D}$$

where D is the dipole strength and R is the rotational

strength of the transition. For a particular vibrational transition between the ground state and some excited state

$$g = \frac{4R}{D} = \frac{4\mathrm{Im} \langle \Psi_0(q,Q)|\mu|\Psi_f(q,Q)\rangle . \langle \Psi_f(q,Q)|m|\Psi_0(q,Q)\rangle}{\mathrm{Re} \langle \Psi_0(q,Q)|\mu|\Psi_f(q,Q)\rangle \langle \Psi_0(q,Q)|u|\Psi_f(q,Q)\rangle}$$

where μ and m are the electric and magnetic transition dipole moment operators, respectively, Ψ_0 and Ψ_f are the ground and excited state wavefunctions, and q and Q refer to the electronic and nuclear coordinates. The excited vibrational state belongs to the electronic ground state manifold.

This result is found by assuming that the material being investigated consists of non-interacting molecules, and follows Beer-Lambert's law (51). Under these circumstances the total absorption depends on the intensity of the radiation used and on the properties of the individual molecules. The theoretical expression for the probability of an absorption taking place in unit time is the product of the radiation density, $I(\tilde{\nu})/c$, and the Ein-

stein probability coefficient for absorption, B. Note that the Einstein coefficient expresses the *total* absorption.

The following is a very brief account of the origin of the terms D and R, using B as a starting point (for a thorough discussion see reference 51):

$$B_{0\to f} = \frac{1}{2\pi\hbar^2\nu^2} \left| \langle \Psi_f(q,Q) \left| \sum_j \frac{q_j}{m_j} e^{iK\cdot r_j} (E_U^* \cdot p_j) \right| \Psi_0(q,Q) \rangle \right|^2$$

where the light is described by the wave vector $K = (2\pi\nu/c)E_K$, and E_K is the unit vector in the propagation direction K; E_U is the unit vector in the polarization direction of the light; q_j is the charge on the j'th particle, r its position, and m its mass; p_j is the momentum of the j'th particle; c is the speed of light, and $\hbar$ is Planck's constant over 2π.

In this expression the phase factor, $e^{iK\cdot r_j}$, may be expanded into an infinite converging series:

$$e^{iK\cdot r_j} = 1 + iK\cdot r_j - \tfrac{1}{2}(K\cdot r_j)^2 + \ldots$$

Retaining the first term of this expansion in the expression for B leads to the integral

$$E_U^* \cdot \langle \Psi_f(q,Q) \left| \sum_j \frac{q_j}{m_j} p_j \right| \Psi_0(q,Q) \rangle$$

which may be rewritten as

$$2\pi i\nu \, E_U^* \cdot \langle \Psi_f(q,Q) \left| \sum_j q_j r_j \right| \Psi_0(q,Q) \rangle$$

and leads to the electric transition dipole operator:

$$\mu = \sum_j q_j r_j .$$

The second term in the expansion gives rise to the following integral:

$$\langle \Psi_f(q,Q) \left| \sum_j \frac{q_j}{m_j} (iK \cdot r_j)(E_U^* \cdot p_j) \right| \Psi_0(q,Q) \rangle .$$

Writing $K = (2\pi\nu/c)E_K$ the integral becomes:

$$2\pi i\nu \langle I_f(q,Q) \left| \sum_j \frac{q_j}{m_j c} (r_j)_K (p_j)_U^* \right| I_0(q,Q) \rangle ,$$

where $(r_j)_K$ is the coordinate of r_j in the direction of light propagation, given by E_K, and $(p_j)_U^*$ is the coordinate of p_j in the direction of the electric vector of the light, given by E_U^*. These two terms may be further expanded:

$$(r_j)_K (p_j)_U^* = \tfrac{1}{2}[(r_j)_K (p_j)_U^* - (p_j)_K (r_j)_U^*]$$

$$+ \tfrac{1}{2}[(r_j)_K(p_j)_{U^*} + (p_j)_K(r_j)_{U^*}]$$
$$= \tfrac{1}{2}[(r_j \times p_j)_{K\times U^*}$$
$$+ \tfrac{1}{2}[(r_j p_j)_{KU^*} + (r_j p_j)_{U^* K}]$$

The first term of this result, $\frac{1}{2}[(r_j \times p_j)_{K \times U^*}$, leads to the magnetic dipole transition operator, m, which now must be evaluated in the direction of the magnetic vector of the light, as indicated by the subscript $K\times U^*$. The second term (in the square bracket) leads to the electric quadrupole transition operator, O. These quantities are purely imaginary.

The total absorption, a, may now be written in terms of the square of the sum of the matrix elements of these three transition moments between the initial and final states.

$$a = \frac{4\pi^2 \tilde{\nu}}{hc} n \sum_f g_f(\tilde{\nu}) |E^*_U . u(0f) + (E_K \times E^*_U) . m(0f) + i\pi\tilde{\nu} E_K O(0f) E^*_U|^2$$

where the g's are line shape functions, and n is the complex index of refraction. In the case of isotropic solutions and randomly polarized light the total absorption is adequately described by including only the first

term, the electric dipole transition operator. It has therefore become customary to describe the strength of a transition in this approximation by the dipole strength:

$$D = \mathrm{Re} \langle \Psi_0(q,Q) | \mu | \Psi_f(q,Q) \rangle \langle \Psi_0(q,Q) | \mu | \Psi_f(q,Q) \rangle$$

However, when using circularly polarized light, which also has an imaginary component, all three terms in the sum will contain nonvanishing real and imaginary parts. This has the consequence that the cross terms between $\mu(0f)$ and $m(0f)$ become important (as well as those between $\mu(0f)$ and $O(0f)$). Thus it can be shown that differential absorption in an isotropic sample depends solely on the cross terms between $\mu(0f)$ and $m(0f)$. In analogy with simple absorption the differential absorption is therefore described by the rotatory power, R:

$$R = \mathrm{Im} \langle \Psi_0(q,Q) | u | \Psi_f(q,Q) \rangle \cdot \langle \Psi_f(q,Q) | m | \Psi_0(q,Q) \rangle$$

It follows from this that R is zero in any molecule where the electric and magnetic transition moments are perpendicular. In terms of symmetry such molecules all possess improper axes of rotation, and are said to be achiral. Chiral molecules have no improper rotation axes (See Chapter I).

The dissymmetry factor, g, can now be expressed in terms of R and D, as shown at the beginning of the chap-

ter:

$$g = \frac{E_L - E_R}{\frac{1}{2}(E_L + E_R)} = \frac{4R}{D}$$

(The cross product with the electric quadrupole transition moment operator makes nonvanishing contributions in oriented samples, in magnetically induced circular dichroism, as well as in the measurement of Raman optical activity.)

Models Describing Vibrational Circular Dichroism.

Although we now know in principle how to find R and D we meet with the familiar problem of not knowing the complete wavefunctions. The usual approach under these circumstances is to separate the wavefunction into the electronic and the nuclear parts, i.e., to invoke the Born-Oppenheimer approximation and put

$$\Psi_0 = Y_G X_g$$

$$\Psi_f = Y_G X_e$$

where Y is the electronic and X the nuclear wavefunction, G and g refer to the ground state, and e to the excited state. The excited nuclear state, X_e, belongs to the

electronic ground state manifold (52).

To get the matrix elements of the magnetic and electric transition dipole operators with respect to these wavefunctions the operators are separated into their electronic and nuclear parts:

$$\mu = \mu_{el} + \mu_n \qquad m = m_{el} + m_n$$

The next step is to find the matrix elements of these operators with the electronic or nuclear wavefunctions, as appropriate. A problem arises, however, when we try to calculate the electronic contribution to the magnetic moment:

$$< Y_G \,|m_{el}|\, Y_G >$$

which vanishes because Y, within the Born-Oppenheimer approximation, is nondegenerate and therefore can be chosen to be real, and m_{el} is an imaginary Hermitian operator. This corresponds to saying that the motion of the electrons have no impact on the magnetic moment of the molecule.

To get around this problem there are several possible approaches, as pointed out by Stephens (52):

1) Ignore the problem and work with the nuclear contribution to the magnetic moment only.

2) Make some modification to the expression for m and μ

such that these quantities treat the electronic contribution implicitly, and then use the Born-Oppenheimer approximation.

3) Rewrite the expression for R in such a way that the magnetic moment is described in some way not involving m, and then invoke the Born-Oppenheimer approximation.

4) Make modifications to the wave functions, i.e., treat the break down in the Born-Oppenheimer approximation directly.

In the following the main principle of each of the models in each group is described very briefly.

1) Cohan et al first identified the problem of the vanishing electronic contribution (53). They ignored it in their calculations. If this had been a successful approximation no other models would have been necessary.

2) In one of the most widely used models, the fixed partial charge model (FPC), μ_{eff} and m_{eff} are calculated from partial charges assigned to the atoms. The charges are independent of the nuclear position, and the μ_{eff} and m_{eff} arise as the nuclear masses move. This model was adapted by Schellman (9) and Deutsche and Moscowitz (7,8) from work done in electronic CD.

The Charge Flow model is an extension of the FPC model in that the assigned charges are allowed to be redistributed during a vibration (54).

The Bond Dipole model (BD) expresses the dipole mo-

ments as the sum of the moments of each bond, or in some cases of groups. The individual moments are functions of the nuclear displacements from equilibrium (55).

3) The models belonging to this group have one thing in common: each apply only in specially defined situations. While they may be useful and successful in those situations, their development reflects the frustrations of trying to find a model which can be used in all instances.

The Coupled Oscillator model considers the interaction between two identical or near identical polar bonds as oscillating dipoles whose interaction gives rise to negative-positive or positive-negative VCD signals of geometry dependent magnitude and wavelength (22).

The Dynamic Polarization model used in electronic CD has been used successfully by Barnett et al to describe the VCD spectra of some transition metal complexes, but its usefulness is limited to such complexes (56).

Barron and Buckingham developed the Inertial Motion model for predicting the intensities of the torsional modes of CH_3 groups (57).

The last model in this group, the Ring Current model, attempts to account for the unusually large VCD signal observed in the carbon-hydrogen stretching region of some molecules, especially the $C_{\alpha}{}^{*}H$ stretching mode of amino

acids. In this model the magnetic moment is shown to be enhanced during the stretching motion by the redistribution of electrons in the ring formed as the carboxylate end of the molecule forms an intramolecular hydrogen bond with the amide end (58).

4) Nafie and coworkers have developed two models which include correction terms to the Born-Oppenheimer approximation: The Localized Molecular Orbital theory adds velocity dependent terms to the Born-Oppenheimer approximation which, while not very important in the IR absorption, strongly influence the VCD intensities of the molecule (59, 60). In the second model a formalism is developed which uses Atomic Polar Tensors to calculate VCD intensities (61).

The most rigorous model to date is probably Stephens's Nonadiabatic Theory. This includes corrections to the Born-Oppenheimer wavefunctions with terms that take into account the electronic motion during a nuclear vibration (62). While this model promises to be universally applicable the calculations are very time consuming and have only been performed on small molecules.

It is worth noting here that any rigorous calculation of a VCD spectrum automatically would include an accurate prediction of the infrared spectrum, frequencies as well as intensities. Considering that normal coordinate calculations for predicting vibrational frequencies still

largely depend on empirically refined force fields, and that the problem of calculating the dipole strength and therefore IR intensities has not yet been solved satisfactorily, it is not surprising that so many, very different models have been developed for the prediction of VCD. Although the work of Stephens's group is impressive it is going take a lot of careful work, and probably a new generation of computers, before their method can be used routinely in the interpretation of spectra. Therefore the less rigorous methods will continue to be useful for a long time.

The Coupled Oscillator.

There are several reasons for choosing to explain the Coupled Oscillator model in detail: The model was used before any VCD had actually been observed to predict which molecules would be good candidates (i.e., have large VCD intensities) for early observation of the weak VCD signal. Thus Holzwarth used the model to predict that diketopiperazine would have a VCD signal at about 1106 cm^{-1} (22). Secondly, the derivation of the model is simple and provides a clear picture of the potential usefulness of VCD for determining molecular conformations. Finally, our group has successfully used the model to correlate the solution conformation of alanyl-alanyl-alanine and DNA to the observed C=O stretching intensi-

ties of these molecules (63, 64). It has also been shown that it is possible to explain the amide III vibrations of alanyl-alanine via this model (65).

In the coupled oscillator model the magnetic dipole moment is expressed in terms of the electric dipole moment and vectors describing the geometry of the system. (The following closely follows the derivation of the coupled oscillator model by Holzwarth and Chabay in reference 22).

Consider two identical diatomic molecules, a and b. The vector T connects their centers of mass, as shown in Fig. 1. The total wavefunctions for the ground- and excited states of each molecule may be written as:

$$\Psi_{a0}(q,Q) \quad \text{and} \quad \Psi_{af}(q,Q) \text{ for a,}$$

and $$\Psi_{b0}(q,Q) \quad \text{and} \quad \Psi_{bf}(q,Q) \text{ for b,}$$

where q and Q stand for electronic and nuclear coordinates, respectively. The total wavefunction for the ground state of the dimer may then be written

$$\Omega^{0}(q_a, q_b, Q_a, Q_b) = \Psi_{a0}(q,Q)\,\Psi_{b0}(q,Q)$$

Because the two molecules are identical the excited state wavefunctions $\Psi_{a0}\,\Psi_{bf}$ and $\Psi_{af}\,\Psi_{b0}$ are degenerate. The excited state wavefunctions of the dimer therefore con-

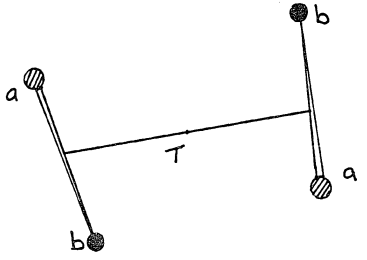

Figure 1. Two identical diatomic molecules, a and b. Their centers of mass are connected by the vector T.

sist of the symmetrically and antisymmetrically coupled functions of the monomer (indicated by + and - respectively).

$$\Omega^{\pm} = (\Psi_{af} \Psi_{b0} \pm \Psi_{a0} \Psi_{bf})/\sqrt{2}$$

Since the VCD signal as previously stated is given by

$$g = \frac{4R}{D} =$$

$$\frac{4\mathrm{Im} < \Psi_0(q,Q)|\mu| \Psi_f(q,Q)>.< \Psi_f(q,Q)|m| \Psi_0(q,Q)>}{\mathrm{Re} < \Psi_0(q,Q)|\mu| \Psi_f(q,Q)>< \Psi_0(q,Q)|\mu| \Psi_f(q,Q)>}$$

we need in our case to find μ and m for the transitions $\Omega^0 \longrightarrow \Omega^-$ and $\Omega^0 \longrightarrow \Omega^+$.

The Electric Transition Dipole Moment.

This is given by

$$\mu^{\pm} = < \Psi_{af} \Psi_{b0} \pm \Psi_{a0} \Psi_{bf}|\Sigma_i e_i y_i + \Sigma_j e_j y_j|\Psi_{a0} \Psi_{b0}>/\sqrt{2}$$

where e is the charge on particle i, and y is the position vector; i refers to monomer a and j to monomer b. If the origin of y is chosen to be the center of mass of the

dimer, and T is the distance vector from the center of mass of a to the center mass of b, we can write the position of particle i with reference to the center of mass of the dimer and the center of mass of the monomer as

$$y_i = r_i - \tfrac{1}{2} T$$

where r is the position vector in monomer a. Similarly for j in monomer b

$$y_j = r_j + \tfrac{1}{2} T$$

The electric dipole moments, $\mu+$ and $\mu-$, may now be written as

$$\mu^{\pm} = (\mu_a \pm \mu_b)/\sqrt{2}$$

where

$$\mu_a = \langle \Psi_{af} | \sum_i e_i r_i | \Psi_{a0} \rangle$$

The frequencies of the two states will be given by

$$\nu^{\pm} = \nu_0 \pm \nu_{ab}$$

where ν_0 is the frequency of the monomer signal and ν_{ab} is the dipolar splitting:

$$\nu_{ab} = [\mu_a \cdot \mu_b / T^3] - [3(\mu_a \cdot T)(\mu_b \cdot T) / T^5] \quad (66)$$

The Magnetic Transition Dipole Moment.

Using a similar procedure as for the electric transition dipole moment m+ and m- may be written

$$m^{\pm} = \frac{\langle \Psi_{a0}\,\Psi_{b0} \mid \sum_i e_i y_i x p_i/g_i + \sum_j e_j y_j x p_j/g_j \mid \Psi_{af}\,\Psi_{b0} \pm \Psi_{a0}\,\Psi_{bf} \rangle}{c(8)^{\frac{1}{2}}}$$

where p is the momentum operator and g the mass. Using the same arguments as before the magnetic transition dipole operator may be written

$$\sum_i e_i(r_i - \tfrac{1}{2}T)x p_i/2cg_i + \sum_j e_j(r_j - \tfrac{1}{2}T)x p_j/2cg_j$$

The sums may be further separated into a term which corresponds to the monomer magnetic dipole transition moment, i.e., for a

$$m_a = \sum_i e_i r_i x p_i/2cg_i$$

and a term involving the distance vector

$$\sum_i (-e_i\ \tfrac{1}{2}T x p_i/2cg_i)$$

For the stretching vibration of the monomer the magnetic transition moment is zero. The transition dipole for the distance term is

$$Tx < \Psi_{af}\,\Psi_{b0} \pm \Psi_{a0}\,\Psi_{bf} | \Sigma_i e_i p_i / g_i | \Psi_{a0}\,\Psi_{b0} >$$
$$\text{---------------------------------------}$$
$$c(8)^{\frac{1}{2}}$$

In the next step the elements in p are substituted by elements in μ (67, 68).

$$Tx\,(-2\pi i\nu) < \Psi_{af}\,\Psi_{b0} \pm \Psi_{a0}\,\Psi_{bf} | \Sigma_i e_i r_i | \Psi_{a0}\,\Psi_{b0} >$$
$$\text{---------------------------------------}$$
$$c(8)^{\frac{1}{2}}$$

where ν is the frequency of the transition of the monomer. This finally allows the magnetic transition dipole moment of the dimer to be expressed in terms of the cross product of the electric transition dipole moments of the monomers

$$m^{\pm} = (-\mu i\nu/2\sqrt{2}c)[Tx(\mu_a \pm \mu_b)$$

From this one may finally write the expression for the VCD transition:

$$g = \frac{4R^{\pm}}{D^{\pm}} = \frac{\mp\, 2(\pi\nu/c)T * (\mu_a x \mu_b)}{\mu^a \pm \mu_a * \mu_b}$$

The Coupled Oscillator model has the immediate advantage of demonstrating clearly that polar achiral groups

in a dissymmetric environment can be expected to display a VCD signal and that the signal itself will carry information about the spatial arrangement of the groups. This is the kind of information which makes VCD so attractive: the conformation(s) of the molecule may in certain instances be deduced from the VCD spectrum. An example of such a situation would be the amide I vibration of a peptide: we already know that the conformation is determined by the conformational angles phi and psi along the backbone of the peptide; since the amide I vibration consists mainly of the C=O stretch these angles may be deduced from the VCD signal in the amide I region, via a CO calculation.

As shown above the model also predicts a split in the vibrational spectrum of such degenerate groups, and a corresponding positive-negative couplet (or negative-positive) in the VCD spectrum. VCD may therefore be helpful in establishing whether a broad poorly resolved signal in the IR spectrum is due to the presence of several conformers of different geometry, or due to splitting caused by identical groups on the same molecule. In the first instance we would expect no VCD signal, in the second we might expect to see a bisignate VCD signal. Thus it was found that a D_2O solution of Ala-Ala-Ala has a stable conformer (or several very similar

conformers), since the VCD signal of the amide I' vibration gives rise to such a bisignate signal (63).

The model has obvious limitations: it is calculated for an idealized system and it is then inferred that identical groups (bonds) in a molecule may be treated as the two monomers in the model. Secondly the model allows only evaluations of such identical achiral groups, and does not treat the whole spectrum. Finally the model supposes that we have information on the absorption and frequency of the monomer transition.

In spite of these limitations, the model has been useful in several situations (22, 63, 69, 70), and its usefulness has been extended for cases involving near-degenerate and non-degenerate oscillators (71). It has been further extended to include molecules which have more than two groups, namely groups along an infinite polymer (11, 12), as well as a polymer of intermediate length (64).

CHAPTER VI

INSTRUMENTATION

The Dispersive Versus the FT Instrument for the Recording of VCD Spectra.

The first measurements of vibrational circular dichroism were made in the mid- 1970s with dispersive instruments (24, 26). At about the same time commercially available Fourier transform infrared instruments were making their appearance, and it was soon obvious that they are far superior to the dispersive instruments. It is therefore not surprising that much energy has been put into applying the Fourier transform technique to VCD (72 - 75). The oft quoted advantages of the FT-IR technique are the increased light throughput, Jaquinot's advantage, due to the absence of slits, and the spectral multiplexing, Fellgett's advantage, which allows an entire spectrum to be recorded in seconds. Of these, Jaquinot's advantage would seem to be particularly appealing to VCD spectroscopists, since the VCD signal is very small, typically 10^{-4} - 10^{-5} the absorbance of the corresponding IR signal. The FT technique holds great promise, particularly for samples in aqueous solution, where the large background absorption of the solvent has to be overcome.

However, so far that promise has not been fulfilled: although excellent spectra have been recorded with the new technique, there are persistent problems which have yet to be solved (15). The following is a brief account of the problems encountered in adapting the FT-IR technique to the VCD experiment (for a more thorough account see reference 15).

1) A crucial step in the recording of the FT-IR spectrum is the analog-to-digital conversion of the signal. Digital data are necessary in order to transform the spectrum from time to frequency domain via a mathematical algorithm. An analog-to-digital converter with a large dynamic range is required in order to accommodate the large center burst of the signal (when the mirrors of the Michelson interferometer are at equal distances from the sample) with high numerical precision. The amplifier used in conjunction with the converter must also be chosen so as to make full use of the analog-to-digital converter's large range. Since the VCD signal is so much smaller than the IR signal the capabilities of the amplifier-converter unit is pushed to its utmost limit in the acquisition of the FT-VCD spectrum. To overcome the problem less bright sources are chosen, and filters are used to eliminate the center burst. Thus much of Jaquinot's advantage is lost.

2) In the recorded spectrum it is necessary to have a

unique reference point, which is used in the Fourier transform algorithm as well as for co-addition of successive scans. Usually the mathematical algorithm used picks the most intense feature, the center burst, for reference point. For various reasons (see reference 5) the center burst is not necessarily the most intense feature of a spectrum recorded in a VCD experiment, and this therefore has to be identified by the person carrying out the experiment.

3) The retardation of the modulator, which produces the circularly polarized light, remains constant throughout each scan. It is therefore necessary to calibrate the recorded signal to compensate for the difference in circularity over the range probed. (This is not unique to FT-VCD: in most dispersive VCD instruments the PEM has fixed retardation, but in the FT instrument it is so by necessity).

4) It appears that the FT-VCD is prone to absorption dependent artifacts whose origin is not clearly understood. To compensate for this a baseline is constructed either by collecting spectra of a racemic mixture or by adding the spectra of both enantiomers of a molecule. The baseline spectrum obtained by either method is subtracted from the VCD spectrum. At present this is probably the most serious obstacle to FT-VCD becoming a widely used technique, since the enantiomer is not available for most

biological compounds, and it is, in most cases, far too difficult and costly to produce one.

The Optimized Dispersive Instrument.

With these considerations in mind it was decided by this group to design a dispersive VCD instrument in which every consideration would be given to improving the light throughput, and in which special attention would be paid to the problems of the dynamic range in the analog-to-digital conversion step. It was recognized that for the dispersive instrument to have a real advantage over the FT instrument it would have to produce spectra with better signal to noise in a shorter time and preferably with less trouble. It was also recognized that a dispersive instrument cannot produce the high resolution possible with the FT instrument (nor would this instrument be able to keep the resolution constant over the spectral range). Furthermore, it was decided to build the instrument to cover the spectral range which includes the amide I, II and III vibrations, and optimize it for the amide III region, since that region has shown great promise for conformational studies. This would be the first instrument capable of routinely recording spectra in that region.

Optical Layout.

The following is a brief description of our instrument. As seen in Figure 1 the instrument resembles in appearance and layout a modified single beam infrared spectrometer. As already stated it is of utmost importance to have the maximum light throughput; therefore, all optical elements have been carefully chosen with this in mind. Furthermore, the number of optical elements have been kept to a minimum throughout the optical path, in order to minimize light loss due to reflection.

The source is a Nernst glower, which has the advantage of being a small compact source and of not needing a special protective atmosphere. There are two source positions: one allows the source to be imaged onto the 2 mm entrance slit 1:1, the *f*/4 setting; at the other position, the *f*/2 setting, the image is enlarged to fit the entrance slit, which has been opened to 4 mm. The *f*/4 setting is used in the range from 1200 to 1800 cm^{-1} where the 2 mm entrance slit gives a resolution of 5.5 to 14.2 cm^{-1}. From 800 to 1200 cm^{-1} the *f*/2 collection optics are used, and this gives a resolution of 3.1 to 11.0 cm^{-1}. These settings allow the maximum light throughput while maintaining reasonable resolution.

Before reaching the entrance slit of the monochromator the light is modulated by a mechanical chopper at a

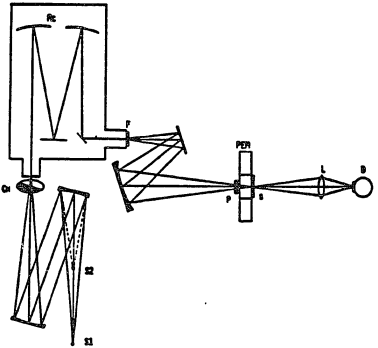

Figure 1. Optical layout of the dispersive VCD instrument. S1 and S2 are the source positions for the f/4 and f/2 configurations, respectively. Ch is the mechanical chopper, Mc the monochromator, F the filter, P the linear polarizer, PEM the photoelastic modulator, S the sample, L the barium fluoride lens, and D the detector.

frequency of 79.5 Hz. The monochromator is a 320 mm focal length Czerney-Turner monochromator with a grating with 120 grooves/mm. All reflective surfaces, including the monochromator grating, are gold coated, since gold has very high reflectivity in the infrared region.

After leaving the monochromator the light passes through a filter in order to remove higher order diffractions (5 - 10 μm or 8 - 15 μm bandpass for the upper- or lower frequency region, respectively). Next, the light passes through a polarizer and a photoelastic modulator (PEM). The polarizer is a gold wiregrid on an AgCl substrate, and it is oriented so that the emerging light is polarized horizontally (this is chosen because the monochromator already has polarized the light somewhat in that direction). The PEM is a single octagonal zinc selenide crystal with antireflective coating. The modulation is produced by piezo-electric quartz drivers, which are oriented at a 45 degree angle to the horizontal. (The PEM is shown separately in Figure 2, and its action will be described below in greater detail). The light is focussed onto the back surface of the PEM. The sample mount is directly behind the PEM, which positions the sample cell so close to the focus that the light goes through a very small volume of the cell. This has the advantage of allowing the use of very small samples, often as little as 7 μL of solution.

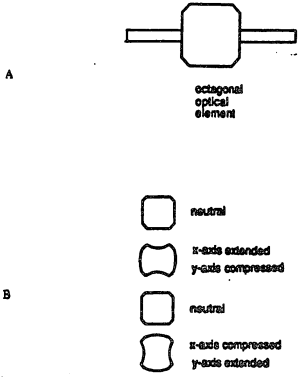

Figure 2. The photoelastic modulator. A) The octagonal ZnSe crystal with two of the quartz drivers (those in the y-direction are not shown). The modulator is oriented so that the plane polarized light enters at an angle of 45° to the drivers. B) shows how the index of refraction is changed alternately in the x and y-direction by the stress produced by the drivers.

The only optical element between the sample and the detector is a barium fluoride lens, thus minimizing possible sources of instrumental birefringence. This focusses the light onto a liquid nitrogen cooled HgCdTe photoconductive detector with an area of 0.5 * 5 mm. The instrument is enclosed in a plexiglass housing, and is purged with dry air, which keeps the relative humidity below 10%. This is done to avoid absorbance due to the water vapor in the atmosphere, which can be large enough at high humidity to obscure the signal sought.

The Photo Elastic Modulator.

The PEM is the heart of the VCD instrument, since it produces the circularly polarized light. Figure 3 shows a schematic of the action of the PEM. A linearly polarized wave can be decomposed into two linearly polarized waves at 45° angles to the original wave, and in phase. When traversing a material which does not have the same refractive index in the two directions of the incident waves the two waves will emerge from the material out of phase. If the thickness of the material is such that one wave is exactly 90° out of phase with the other, the combination of the two waves will be a circularly polarized wave. Such a quarter wave plate will only be effective for one particular wavelength (3). The PEM acts by

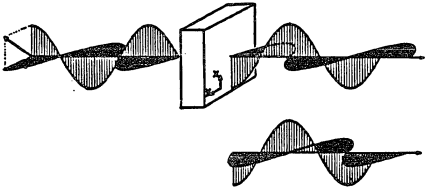

Figure 3. Quarter wave plate. The plane polarized light enters the crystal at an angle of 45° to the x and y-directions. The refractive index is not the same along the two coordinates; therefore the two component waves emerge from the crystal out of phase. If the phase difference is exactly 90° the light is circularly polarized.

stress birefringence: the difference in refractive index is produced by pressure applied by the quartz drivers. This has two advantages; first it possible to change the stress very rapidly from one direction to another at 90° to the original direction, thus producing alternately right- and left circularly polarized light; secondly, the stress can be varied by varying the electric signal to the quartz drivers so that it is possible to produce light which is circularly polarized over a large range of frequencies. In our instrument the signal to the drivers is recalculated for each wavenumber so that the light is always circularly polarized. The PEM changes between right - and left circularly polarized light at a frequency of 31.2 kHz.

The HgCdTe Detector.

As mentioned earlier the VCD instrument was explicitly designed for use in the frequency region of the amide I - III vibrations. This is primarily determined by the choice of detector, which in this case was chosen to work at its optimum between 800 and 1500 cm^{-1}. The response of a detector to the incident light is expressed in terms of its detectivity, D^* (76). The maximum D^* of the detector in the VCD unit is $3.5*10^{10}$ cm $Hz^{\frac{1}{2}}/W$ (77). The response over the spectral range is shown as a percentage of the

maximum D^* in Figure 4. It is highest around 900 cm^{-1} and stays at or above 50% for the region between 800 and 1500 cm^{-1}. Below 800 cm^{-1} the response drops off rapidly, but in the region from 1500 to about 2100 cm^{-1} the response is still about 40% which allows some strong signals to be detected. Detection of signals below 800 cm^{-1} is also limited by the barium fluoride lens used in the design, which is not transparent below 800 cm^{-1}.

The Nature of the Detected Signals.

The detected signal is doubly modulated: at 79.5 Hz, the frequency of the mechanical chopper, and at 31.2 kHz, the frequency of the PEM. By tuning a lock-in amplifier to 79.5 Hz one obtains a dc signal, I_{DC}, which corresponds to the total transmission; by tuning in to the PEM frequency one obtains an ac signal, I_{AC}, which contains the VCD information. The differential absorption, ΔA, is given by

$$\Delta A(\tilde{\nu}) = k \frac{I_{AC}(\tilde{\nu})}{I_{DC}(\tilde{\nu})}$$

where k is a constant. For small values of $I_{AC}(\tilde{\nu})/I_{DC}(\tilde{\nu})$ k is approximately equal to 1.15 (See reference 5, which also deals with larger values of

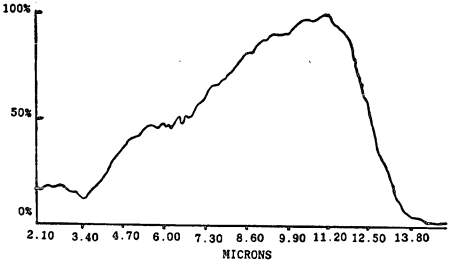

Figure 4. Detector response over the spectral range as a percentage of the maximum response. As indicated the spectral response is over 50% between 800 and 1500 cm^{-1}.

$I_{AC}(\tilde{\nu})/I_{DC}(\tilde{\nu})$).

To avoid having to worry about the exact concentration of samples it has become common practice to report the value as $\Delta A/A$. This is particularly useful when very small sample volumes are prepared, and also eliminates the worry about solvent evaporation when the sample cell is filled. This is justified for samples obeying Beer-Lambert's law since, in that situation, the molar absorptivity, E, is given by

$$E = \frac{A}{C\,l}$$

where C is the concentration in moles per liter, and l is the pathlength in centimeters. In that case the dissymmetry factor, g, is given by

$$g = \frac{\Delta E}{E} = \frac{\Delta A}{A}$$

Electronic Layout.

Figure 5 shows the layout of the electronic circuit of the VCD instrument. Immediately after leaving the detector the signal is fed through a preamplifier, after which it is split into two paths: one path leads through a lock-in amplifier tuned to 79.5 Hz. The output of this amplifier is I_{DC}, which is read by the computer. The

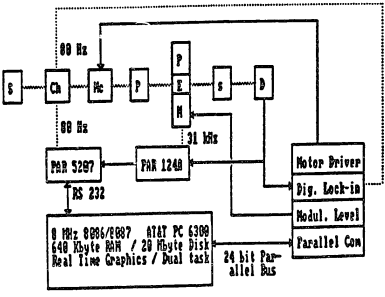

Figure 5. Electronic layout of the VCD instrument. The same symbols are used as in figure 1. PAR 5207 and PAR 124A are lock-in amplifiers from Princeton Applied Research.

other path leads to a lock-in amplifier tuned to the frequency of the PEM (31.2 kHz). The output of this amplifier now carries the VCD information (I_{AC}) modulated at the frequency of the chopper. The next step is the demodulation of the 79.5 Hz signal and the subsequent conversion from analog to digital signal: this is the crucial step referred to in 1) above. Both lock-in amplifiers used in the monitoring of the I_{AC} signal have been carefully selected so as to accommodate the large dynamic range. Since there is more time available than in an FT-VCD experiment (the acquisition cycle is simply interrupted) it is possible, via the computer, to recalculate and change the setting for the second amplifier so that the analog-to-digital conversion step always takes place under optimum conditions. Thus the problem of dynamic range is overcome.

The fact that the dispersive instrument collects the data consecutively over the frequency range allows the voltage to the PEM to be recalculated to give a retardation of $\pi/2$ for each data point. Thus the light is always circularly polarized, and the ΔA value may be calculated directly from the I_{AC} and I_{DC} values without any need for calibration.

The instrument is completely computer driven, with the exception of the changing of slitwidth and filter, and the positioning of the optical elements and the detector.

The computer also has the necessary programs for averaging and smoothing, subtracting background spectra and plotting. Furthermore, the instrument is simple to run and most spectra are recorded in a few hours (usually 20 averaged spectra). Maintenance is also very simple, consisting mainly in changing the source, which burns out after six months to a year.

CHAPTER VII

VIBRATIONAL CIRCULAR DICHROISM OF ALANYL-ALANINE AND ITS ISOTOPOMERS.

Background.

Until the time of the study reported here VCD intensities had been observed for the amide A, I, and II vibrations in poly(amino acids) and small peptides (78 - 85). Most of these studies were of non-aqueous solution (78, 80 - 83). This study presents the first ever observation of VCD in the amide III region in aqueous solution (47). A detailed analysis of the results will be carried out with references to the work already discussed in chapters II - IV.

Previous Raman studies of the amide III vibrations have shown differences in intensity and frequency in this region for different secondary structures of poly(amino acids) or peptides (44). As already mentioned during the discussion of the normal coordinate analysis a similar effect, although small, is observed for the dipeptide L-Ala-L-Ala and its diastereomer D-Ala-L-Ala (Chapter IV, Figure 1). Since the difference between the two diastereomers consists merely of the interchange of a methyl

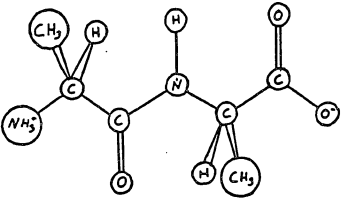

A

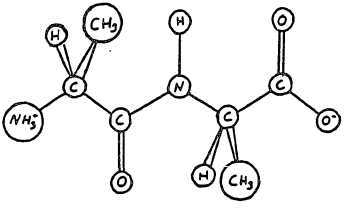

B

Figure 1. A) L-alanyl-L-alanine.
B) D-alanyl-L-alanine.

group and a hydrogen on one of the chiral carbons (Figure 1) this observation suggests that there may also be a conformational difference between the diastereomers. The study of alanine has shown that the two methine deformations give rise to large VCD signals (86), and it was therefore expected that this would also be the case for those alanyl dipeptide modes which involved the methine deformations. Since it was shown that the amide III modes are due to extensive mixing of the C^{*}-H and the N-H deformation coordinates (see Chapter IV) it was thought that the VCD signal of these modes would in some way reflect the structural difference, as well as any possible conformational differences. The vibrational analysis of L-Ala-L-Ala provides a solid background for the interpretation of the VCD of the alanyl dipeptides in the region containing the amide I, II, and III modes, i. e., from approximately 1200 - 1750 cm^{-1}.

Experimental.

As discussed in the previous chapter, the choice of detector largely determines the optimum range of the instrument. There are, however, two other factors which determine the accessibility of a region: the material used for the windows of the sample cell, and the choice of solvent. Since the signal is so small it is essential that the windows are made of a material which has very

low refractive index to minimize the loss of light due to reflection at the interfaces. The best choice is CaF_2, which has a refractive index of 1.4 at 5μm and is very slightly soluble in water. CaF_2 cuts off at about 1050 cm^{-1}; thus for spectra below 1050 cm^{-1} BaF_2 windows, which cut off at about 800 cm^{-1}, may be used. BaF_2 has a refractive index of 1.45 at 5μm, slightly higher than CaF_2, but more importantly, it is about a hundred times more soluble. Therefore CaF_2 is used whenever possible. (The solubility of CaF_2 is app. 0.0017 gm / 100 mL at 26° C, and BaF_2 app. 0.12 gm / 100 mL at 26° C) (87).

As already indicated the solvents used were H_2O and D_2O, which are not generally considered to be good solvents for IR studies: H_2O absorbs strongly from ca. 1550 - 1750 cm^{-1} and D_2O from ca. 1150 - 1250 cm^{-1}, Figure 2. In addition, there is strong background absorption outside the absorption peaks, which is particularly strong at frequencies below the absorption peaks, and stronger in H_2O than in D_2O. Although the D_2O background is somewhat weaker at the frequencies above the absorption peak, the lower response of the detector limits the light detected. This makes it difficult to work at pathlengths of more than 15 μm. Consequently, H_2O was used as solvent for spectra from 1250 - 1500 cm^{-1} and D_2O from 1450 - 1750 cm^{-1} with pathlengths of 15 μm.

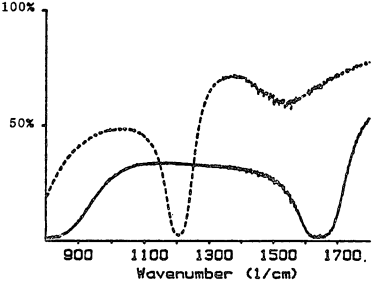

Figure 2. IR transmission spectra of H_2O (solid trace) and D_2O (broken trace), from 800 - 1800 cm^{-1}, using a cell with BaF_2 windows and a 15 um spacer.

The alanyl dipeptides, L-Ala-L-Ala, D-Ala-D-Ala, L-Ala-D-Ala and D-Ala-L-Ala, were all commercially available and were bought from either Chemical Dynamics Corp. or Research Plus, Inc. They were used without further purification. In addition, a sample of L-Ala-d_1-L-Ala was synthesized by the method described in Chapter II.

For solutions in D_2O the peptide was first dissolved in D_2O and evaporated to dryness in a lyophylizer or rotovap to exchange the labile protons with deuterium before the final solution was made up. In accordance with the notation introduced by Miyazawa et al (46) the amide vibrations of the deuterated samples are referred to by a prime (e.g. amide I'). The concentrations of the H_2O solutions were 1 M and the D_2O solutions were 0.5 M.

The spectra of L-Ala-L-Ala, D-Ala-D-Ala, L-Ala-D-Ala and D-Ala-L-Ala were collected with a scan speed of 1 cm^{-1} / s and a time constant of 1 s. The slitwidth was constant at 2 mm which meant a bandpass of 4-8 cm^{-1}, depending on the frequency. The pathlength, as already mentioned, was 15 um. Usually 10 VCD spectra were collected and averaged. The spectra of L-Ala-d_1-L-Ala were collected at a later date when the instrument was set up with a different configuration of collection optics. Therefore the slitwidth was 3 mm with a bandpass of about 8-12 cm^{-1}. This allowed sufficient light to make it

possible to use a pathlength of 25 μm for the solution in D_2O. For this sample 20 spectra were collected and averaged.

It is virtually impossible to design an instrument which is completely free of induced artifacts. Since the measured signal is so small, any instrumental birefringence shows up as a "background" signal in the spectrum. To compensate for this, a background spectrum was constructed. The VCD spectra of two enantiomers are exact mirror images of each other, provided the experimental conditions are the same; therefore the average of two such spectra should be zero, and any intensity left after the averaging may be assumed to be due to instrumental artifacts. Therefore the background spectrum was constructed by taking ten spectra of each of the enantiomeric pair and averaging all twenty spectra. The background thus constructed was subtracted from the averaged VCD spectrum. This procedure was followed for the original work on the alanyl dipeptide described in reference 47. Later it was found that the average spectrum of the solvent alone taken with the same instrument setting as used in the collection of the sample VCD spectra provides a very good background. Thus in the case of the L-Ala-d_1-L-Ala the solvent spectrum was used for background subtraction.

Results and Discussion.

The Amide III Region.

The IR and VCD spectra of the diastereomers L-Ala-L-Ala (solid trace) and L-Ala-D-Ala (broken trace) between 1250 and 1500 cm^{-1} are shown in Figure 3. Inspection immediately reveals that the difference between the diastereomers observed in the Raman spectrum is also clearly observable in the IR spectrum. Furthermore, the VCD spectrum of L-Ala-L-Ala shows a large positive peak corresponding to the most strongly coupled of the amide III features, namely amIII,1 at 1280 cm^{-1}, and a smaller negative feature corresponding to amIII,2, at 1325 cm^{-1}, whereas the spectrum of L-Ala-D-Ala shows a large negative feature for the amIII,1 and a smaller positive feature for amIII,3, at 1340 cm^{-1}. These significant differences between the VCD spectra of the two diastereomers immediately suggest that it is the extensive coupling observed in this region which gives rise to different VCD signals for the two diastereomers.

To obtain the full benefit of the knowledge gained by the vibrational analysis and the normal coordinate calculations described in chapter IV, the VCD spectra of the amide III region of the species analyzed there will first be examined. Later the spectra of the available diastereomers will be examined and the analysis completed. In the following, references will be made in brackets to Figure

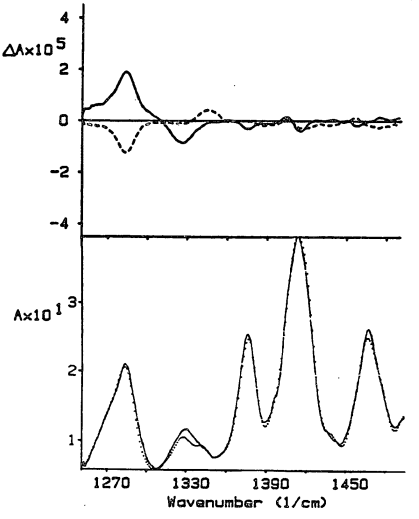

Figure 3. VCD (top) and IR spectra (bottom) of L-Ala-L-Ala ——— and L-Ala-D-Ala ----- in H_2O between 1250 and 1500 cm^{-1}.

2 Chapter IV. To facilitate the comparison all spectra have been plotted to the same scale, and all frequencies and intensities have been summarized in Table I.

One of the molecules, the fully deuterated species, L-Ala-d_1-L-Ala-d_1 (trace A and B), was not available. This molecule in D_2O (CDNDCD, trace A) has no vibrations in the region and therefore can not have any VCD spectrum. The same molecule in H_2O (CDNHCD, trace B) shows the "unperturbed" amide III vibration. Although it would have been nice to have the VCD spectrum of this it would almost certainly have shown only a very weak VCD signal solely due to the chiral perturbation of the "unperturbed" amide III mode, as no chiral atom is directly involved in the vibration, and there is no evidence of any transition dipole coupling (which might give rise to a "coupled oscillator" signal, described in chapter V). L-Ala-d_1-L-Ala in D_2O (CDNDCH, trace C), shown in Figure 4, is similar to alanine in D_2O, shown in Figure 5, broken trace (86): both have only one methine hydrogen, and there is no perturbing N-H vibration. The frequencies and IR and VCD intensities of alanine have been included in Table I. Although the two methine deformation modes occur about 25 cm^{-1} towards higher frequencies in alanine they are in both molecules separated by approximately 50 cm^{-1}. The low frequency deformation has a positive and

Table I

L-alanine in D_2O			L-ala-di-L-ala in D_2O			L-ala-di-L-ala in H_2O			L-ala-L-ala in D_2O			L-ala-L-ala in H_2O			
Obs. freq. cm^{-1}	IR int. A	VCD int. $\Delta\epsilon \times 10^6$	Obs. freq. cm^{-1}	IR int. A	VCD int. $\Delta\epsilon \times 10^6$	Obs. freq. cm^{-1}	IR int. A	VCD int. $\Delta\epsilon$	Obs. freq. cm^{-1}	IR int. A	VCD int. $\Delta\epsilon$	Obs. freq. cm^{-1}	IR int. A	VCD int. $\Delta\epsilon$	Assignment
									1350	0.29	-1.6				C_β-H,2
												1340	0.00	-	AmII,2
						12267	0.01	-							(Am3/CH),2
1343	0.27	-1.5	1333	0.32	-2.7				1333	0.17	-0.9				C_α-H,2*
												1325	0.05	-0.7	AmII,2
						1310	0.05	-0.3							(Am3/CH),1
									1307	0.05	0.9				C_β-H,1
1297	0.17	1.6	1301	0.14	4.4	1281	0.03	1.2	1281	0.10	2.9				C_α-H,1*
												1280**	0.15	1.8	AmIII,1

Frequencies, and IR and VCD absorbance of all L-Ala-L-Ala analogues and of alanine in the amide III region. * also refers to the C^*-H modes of alanine. ** this assignment was based on a band decomposition.

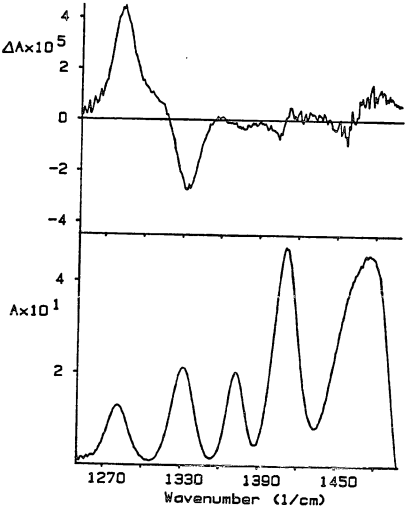

Figure 4. VCD (top) and IR spectra (bottom) of L-Ala-d_1-L-Ala in D_2O between 1250 and 1500 cm^{-1}. Note the similarity of the couplet to that observed in alanine, Figure 5.

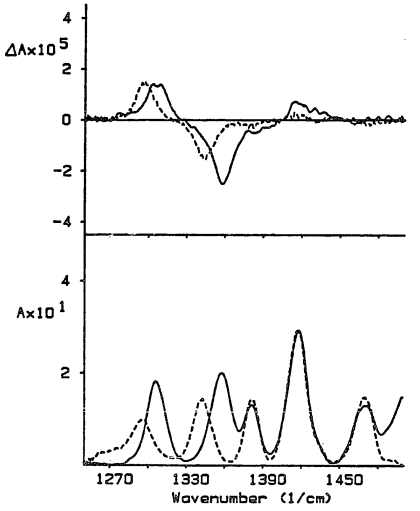

Figure 5. VCD (top) and IR (bottom) spectra of L-alanine in H_2O ——— , and in D_2O ---- between 1250 and 1500 cm^{-1}.

the high frequency deformation a negative VCD signal in both instances, but the intensity of the dipeptide signal is about twice that of the amino acid. It is worth reminding oneself that although there is a positive and a negative signal this is not a couplet such as might be expected from coupled vibrations; these are two separate signals due to the two near degenerate perpendicular deformation modes of one bond.

Comparing this to L-Ala-d_1-L-Ala in H_2O (CDNHCH, trace D), shown in Figure 6, solid trace, the low frequency positive signal of the C_α-H,1 deformation is still seen, but the intensity of the signal is much lower. This methine deformation was shown in the normal coordinate calculations to take only a small part in the coupling with the N-H deformation, but it was stressed that the nature of this mode is different from the C_α-H,1 mode in the molecules where no N-H group is present; it is therefore not inconsistent that the VCD signal is much smaller. It would have been very convincing if there had been a couplet at 1311 and 1346 cm^{-1}, corresponding to the coupled vibrations, (Am3/CH),1 and (Am3/CH),2, but unfortunately there is only a small negative signal at 1319 cm^{-1} and no signal large enough to interpret at a higher frequency. However, judging from the two spectra just described (alanine in D_2O and L-Ala-d_1-L-Ala in D_2O), one would definitely expect to see a large negative signal at

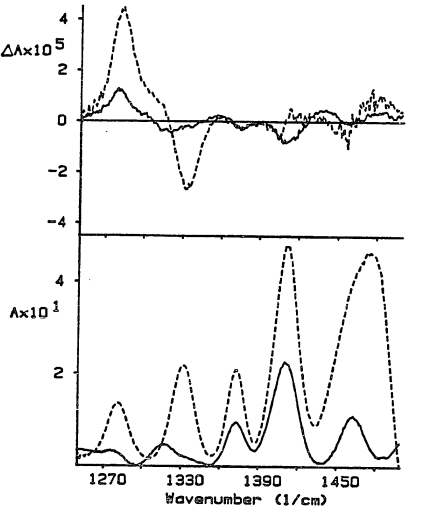

Figure 6. VCD (top) and IR (bottom) spectra of L-Ala-d_1-L-Ala in H_2O ——— between 1250 and 1500 cm^{-1}. The spectrum of the molecule in D_2O ----- has been included to emphasize that there is no signal in the undeuterated molecule corresponding to the large negative signal observed in the deuterated species.

approximately 1330 cm^{-1}, due to the second methine deformation, if there was no interaction between this and the N-H deformation. Thus the lack of signal at this frequency may be seen as a confirmation of the existence of coupling between the two coordinates, especially when it is remembered that the intensity of coupled signals is highly dependent on the relative positions of the coordinates taking part in the coupling (strictly speaking it depends on the directions of the transition moments, which are related to the direction of the coordinates).

The IR and VCD spectra of L-Ala-L-Ala in D_2O (CHNDCH, trace E) are shown in Figure 7. The VCD spectrum is interpreted as follows: the positive and negative features of the two orthogonal C_O-H deformations are seen at 1281 and 1333 cm^{-1}, respectively. In addition to these, and partly overlapping them, the two C_N-H deformations, a positive and a negative feature, are seen at 1307 and 1360 cm^{-1}, respectively. The C_N-H,1 vibration has a very small IR intensity, but was clearly identified in the Raman spectrum.

Figure 3, solid trace, shows the IR and VCD spectra of the last molecule in this series: L-Ala-L-Ala in H_2O (CHNHCH, trace F). The difficulty in interpreting the VCD spectrum in the amide III region of this molecule stems from the fact that there are three overlapping spectral

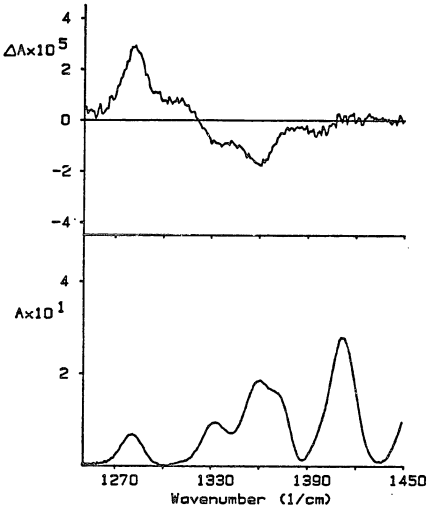

Figure 7. VCD (top) and IR (bottom) spectra of L-Ala-L-Ala in D_2O between 1250 and 1500 cm^{-1}.

IR features in the region covered by the large positive VCD signal centered around 1280 cm^{-1}. From the above analysis it becomes apparent that both the C_O-H,1 and the C_N-H,1 must be contributing to the signal (these are the two coordinates which did not take part in the coupling in the amide III region, see Chapter III). This leaves the question of a possible contribution from the very large highly coupled feature observed in the IR, namely amIII,1. There are several reasons for believing that this coordinate does make a significant positive contribution to the VCD signal at 1280 cm^{-1}:

a) The above analysis has shown that C_O-H,1 and C_N-H,1 only overlap partly, whereas the present signal appears as one large feature.

b) It was found in the normal coordinate calculations that C_O-H,1 in L-Ala-L-Ala in H_2O was most similar to the C_O-H,1 in L-Ala-d_1-L-Ala in H_2O, and it was shown above that the latter gave rise to a VCD signal of an intensity considerably smaller than that which is observed in the present signal.

c) The smaller negative feature at 1325 cm^{-1} corresponding to another of the highly coupled features, amIII,2, is believed to be coupled to the larger positive feature via a coupling mechanism similar to that of coupled oscillators (see below).

The last statement is partly based on a comparison

between L-Ala-L-Ala and one of its diastereomers, L-Ala-D-Ala. The spectra of these two molecules in D_2O will first be compared, Figure 8 and Table II. The solid trace refers to L-Ala-D-Ala. Since the chirality of the carbon at the carboxylate end of the molecule is changed the signs of the C_O-H signals have changed, as expected. Also as expected the C_N-H,1 signal has retained its sign and magnitude, but the C_N-H,2 signal in L-Ala-D-Ala has disappeared.

In H_2O the spectra of L-Ala-L-Ala and L-Ala-D-Ala are very different (Figure 3). In L-Ala-D-Ala the low frequency peak has changed sign and is smaller and slightly differently shaped. There is no signal corresponding to amIII,2 but a small positive signal corresponding to amIII,3 at 1343 cm^{-1}. The difference in shape of the low frequency VCD signal is partly due to the fact that the C_N-H,1 signal does not change sign. The C_O-H,1 signal is expected to be negative, and the amIII,1 signal is also negative, although not necessarily of the same magnitude as in L-Ala-L-Ala. However, it is only by considering the signals in this region to be due to a coupling mechanism that the different appearances of the signals in the two diastereomers can be adequately explained: the slightly different environments of some of the atoms in the diastereomers cause a difference in the coupling pattern in

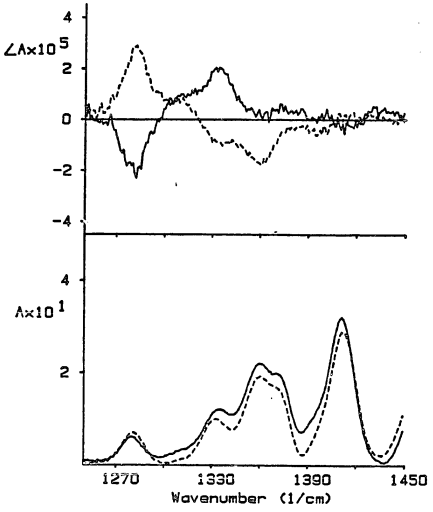

Figure 8. VCD (top) and IR (bottom) spectra of L-Ala-D-Ala in D_2O ——— between 1250 and 1450 cm^{-1}. The spectra of L-Ala-L-Ala in D_2O have been included for comparison, -----.

Table II

L-Ala-L-Ala in D_2O			L-Ala-D-Ala in D_2O			L-Ala-L-Ala in H_2O			L-Ala-D-Ala in H_2O			Assignment
Obs. freq. cm^{-1}	IR int. A	VCD int. $\Delta A \cdot 10^5$	Obs. freq. cm^{-1}	IR int. A	VCD int. $\Delta A \cdot 10^5$	Obs. freq. cm^{-1}	IR int. A	VCD int. ΔA	Obs. freq. cm^{-1}	IR int. A	VCD int. ΔA	
1360	0.29	-1.0	1360	0.21	-							C_β-H,R
						1340	0.03	-	1343	0.03	0.4	AmIII,3
1333	0.17	-0.8	1332	0.12	1.9							C_α-H,R
						1325	0.06	-0.7	1322	0.05	-	AmIII,2
1307	0.08	0.0	1307	0.03	0.9							C_β-H,1
1281	0.10	2.9	1281	0.07	-2.1							C_α-H,1
						1280*	0.15	1.8	1280*	0.16	-1.3	AmIII,1

IR and VCD absorbances of the diastereomers L-Ala-D-Ala and L-Ala-L-Ala in H_2O and in D_2O.

the amide III region: in L-Ala-L-Ala the amIII,1 vibration is coupled with amIII,2, and in L-Ala-D-Ala with amIII,3. It has been shown that it is possible to reproduce the spectra observed by considering three coupled oscillators (65). This explanation is in complete agreement with all previous observations and leads to an explanation of the different appearance of the Raman spectra of the two diastereomers, which initially was the reason for this study. It is also possible that the diastereomers have slightly different conformations, a possibility which gains some validity from the disappearance of the C_N-H,2 VCD signal in L-Ala-D-Ala in D_2O.

Normal Coordinate Analysis of the Diastereomers.

Although it was assumed in the normal coordinate analysis that the molecule is present in its extended form it is likely that the coupling patterns are different for the two diastereomers at least partly because of the different geometry around the chiral carbon at the carboxylate end of the molecule. It might therefore prove useful to compare the normal coordinate calculations of the diastereomers.

The difference between the frequencies calculated were less than one wavenumber and the changes in the PED's were 1% or less in the few cases where any changes were seen. The s-vectors were therefore examined to see if the

changes showed up more clearly there. When comparing the s-vectors of an enantiomeric pair their absolute values are identical. This is expected: a normal coordinate analysis is essentially a calculation of the behavior of connected springs of varying lengths, with different force constants and different masses attached to them. If we set up a calculation of a mirror image system, only the sign of some of the displacement coordinates will change; their magnitude will remain the same. This is not the case if one calculates the values for the diastereomers. Three situations arise:

A) a localized vibration, where the mode is completely dominated by the motion of a single coordinate, exhibits s-vector components for which the absolute value is either completely or almost completely identical for the diastereomers. Such is the case for the amide A vibration, which consists almost entirely of the N-H stretch.

B) For more complex vibrations which do not include any significant contribution from atoms attached to the chiral carbons (as for example amide I), the s-vectors are still almost identical. Table III and IV show that the differences do not exceed 0.001.

C) As the vibrations become more complex, with many atoms participating in the motion, this is no longer true. In the heavily coupled amide III region, the differences

Table III

	DEL X	DEL Y	DEL Z
ATOM # 1	.2291	-.0716	-.0034
ATOM # 2	-.1094	.0009	.0001
ATOM # 3	-.0534	.0508	-.0001
ATOM # 4	-.0413	.1248	-.0002
ATOM # 5	.0038	-.0050	.0008
ATOM # 6	.0003	.0007	-.0004
ATOM # 7	.0046	.0137	.0020
ATOM # 8	-.0061	-.0061	-.0003
ATOM # 9	.0011	.0032	.0000
ATOM # 10	.0023	.0006	.0000
ATOM # 11	-.0214	.0139	.0028
ATOM # 12	-.0010	-.0019	.0009
ATOM # 13	-.0327	-.1069	-.0250
ATOM # 14	.0033	.0014	.0008

S-vector of L-Ala-L-Ala amide I vibration.

Table IV

	DEL X	DEL Y	DEL Z
ATOM # 1	.2291	-.0716	-.0034
ATOM # 2	-.1094	.0009	.0002
ATOM # 3	-.0534	.0508	.0005
ATOM # 4	-.0413	.1248	-.0005
ATOM # 5	.0038	-.0050	-.0009
ATOM # 6	.0003	.0007	.0004
ATOM # 7	.0045	.0136	-.0020
ATOM # 8	-.0061	-.0061	.0003
ATOM # 9	.0011	.0032	.0000
ATOM # 10	.0023	.0006	.0000
ATOM # 11	-.0214	.0139	.0028
ATOM # 12	-.0010	-.0019	.0009
ATOM # 13	-.0327	-.1069	-.0250
ATOM # 14	.0033	.0014	.0008

S-vector of L-Ala-D-Ala amide I vibration.

between diastereomeric forms become significant and involve all atoms which take part in the coupling. The differences are now much larger, at approximately 0.02 (Table V and VI).

The normal coordinate analysis gives no direct information about the electric dipole or the magnetic dipole moments. It can therefore only give the frequencies, but not the intensities of the vibrational signals, and it can say nothing directly about the VCD signals. But the coupling patterns in the amide III region do show sufficiently large changes to account for changes of the electric and magnetic dipole moments, with resulting changes in the vibrational and, particularly, the VCD spectra. It may therefore be concluded that in heavily coupled modes involving more than one chiral center large changes in the VCD spectrum can be expected if the chirality of one of the centers is changed, and that such changes will be reflected in the normal coordinate analysis.

The Amide I' and Amide II' Region.

As previously noted only D_2O is transparent in the region between 1450 and 1750 cm^{-1}. This region contains the amide I' and amide II' modes, and the carboxylate anion asymmetric stretch, shown in Figure 9. The amide I' consists mostly of the carbonyl stretch and the amide II' of the N-H in plane deformation, with a small contribu-

Table V

A		DEL X	DEL Y	DEL Z
ATOM #	1	.0047	.0802	-.0407
ATOM #	2	-.0184	-.0055	.0028
ATOM #	3	.0198	-.0385	.0042
ATOM #	4	.0189	-.2807	-.0068
ATOM #	5	.0299	-.0055	.0084
ATOM #	6	-.0031	-.0005	.0030
ATOM #	7	-.1111	.0587	-.0851
ATOM #	8	-.0013	-.0050	-.0081
ATOM #	9	.0034	.0061	.0010
ATOM #	10	-.0044	-.0003	.0010
ATOM #	11	.0256	.0601	.0351
ATOM #	12	-.0079	-.0016	.0104
ATOM #	13	-.3307	-.6998	-.2781
ATOM #	14	-.0049	-.0054	.0058

B		DEL X	DEL Y	DEL Z
ATOM #	1	.0226	.0690	.0135
ATOM #	2	-.0275	-.0034	-.0009
ATOM #	3	.0006	-.0309	.0008
ATOM #	4	-.0009	-.0828	.0073
ATOM #	5	.0745	-.0760	.0409
ATOM #	6	-.0090	.0009	.0124
ATOM #	7	-.4882	.5090	-.3081
ATOM #	8	-.0298	.0056	-.0499
ATOM #	9	.0013	.0101	.0061
ATOM #	10	.0165	.0088	.0061
ATOM #	11	-.0165	-.0377	-.0105
ATOM #	12	.0022	.0008	-.0041
ATOM #	13	.1119	.2303	.0908
ATOM #	14	.0012	.0008	-.0018

C		DEL X	DEL Y	DEL Z
ATOM #	1	.0517	.1228	.0153
ATOM #	2	-.0778	-.0045	-.0013
ATOM #	3	.0351	-.0595	-.0125
ATOM #	4	.0307	-.4519	.0081
ATOM #	5	.0191	.0598	-.0048
ATOM #	6	-.0019	-.0018	.0012
ATOM #	7	.0387	-.4568	-.0268
ATOM #	8	.0179	-.0078	.0240
ATOM #	9	.0045	.0015	-.0026
ATOM #	10	-.0209	-.0042	-.0026
ATOM #	11	-.0232	-.0483	-.0113
ATOM #	12	.0022	.0008	-.0050
ATOM #	13	.1271	.2281	.0988
ATOM #	14	.0011	.0005	-.0015

S-vectors of L-Ala-L-Ala amIII,3 (A), amIII,2 (B), and amIII,1 (C) vibrations.

Table VI

A		DEL X	DEL Y	DEL Z
ATOM #	1	-.0049	-.0803	.0411
ATOM #	2	.0187	.0055	-.0029
ATOM #	3	-.0201	.0388	-.0061
ATOM #	4	-.0194	.2810	.0103
ATOM #	5	-.0310	.0036	.0111
ATOM #	6	.0032	.0002	.0033
ATOM #	7	.1238	-.0381	-.0938
ATOM #	8	.0008	.0052	-.0083
ATOM #	9	-.0035	-.0081	.0011
ATOM #	10	.0049	.0003	.0011
ATOM #	11	-.0254	-.0598	-.0351
ATOM #	12	.0078	.0018	-.0103
ATOM #	13	.3283	.0272	.2770
ATOM #	14	.0048	.0054	-.0058

B		DEL X	DEL Y	DEL Z
ATOM #	1	.0222	.0684	.0131
ATOM #	2	-.0270	-.0034	-.0010
ATOM #	3	.0003	-.0305	-.0044
ATOM #	4	-.0013	-.0806	-.0013
ATOM #	5	.0738	-.0773	-.0399
ATOM #	6	-.0089	.0009	-.0122
ATOM #	7	-.4822	.5206	.3036
ATOM #	8	-.0301	.0056	.0500
ATOM #	9	.0012	.0102	-.0060
ATOM #	10	.0168	.0089	-.0060
ATOM #	11	-.0163	-.0373	-.0105
ATOM #	12	.0022	.0008	-.0041
ATOM #	13	.1111	.2278	.0900
ATOM #	14	.0012	.0008	-.0018

C		DEL X	DEL Y	DEL Z
ATOM #	1	.0522	.1239	.0133
ATOM #	2	-.0785	-.0045	-.0008
ATOM #	3	.0350	-.0695	.0082
ATOM #	4	.0393	-.4634	-.0012
ATOM #	5	.0186	.0878	.0060
ATOM #	6	-.0018	-.0019	-.0010
ATOM #	7	.0468	-.4401	.0207
ATOM #	8	.0175	-.0077	-.0238
ATOM #	9	.0045	.0017	.0026
ATOM #	10	-.0206	-.0042	.0026
ATOM #	11	-.0237	-.0506	-.0109
ATOM #	12	.0023	.0009	-.0053
ATOM #	13	-.1310	-.2457	-.1034
ATOM #	14	.0012	.0006	-.0017

S-vectors of L-Ala-D-Ala amIII,3 (A), amIII,2 (B), and amIII,1 (C) vibrations.

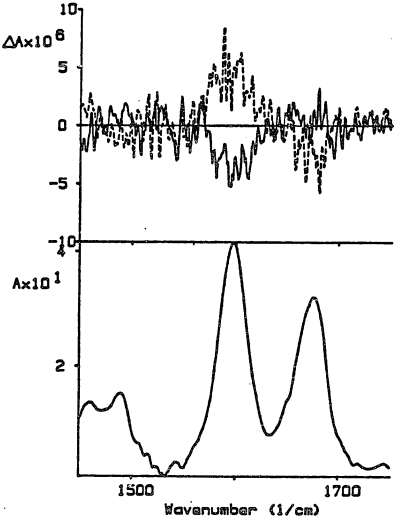

Figure 9. IR spectrum (bottom) of L-Ala-L-Ala from 1450 to 1750 cm^{-1}. VCD spectra (top) of L-Ala-L-Ala, solid trace, and L-Ala-D-Ala, broken trace. The sign of the VCD signal for the carboxylate anion asymmetric stretch reflects the chirality of the terminal residue.

tion from the C-N stretch; thus neither of these modes involve a chiral carbon. The amide vibrations do not give rise to any detectable signal, but the CO_2^- asymmetric stretch gives rise to a very small VCD signal. The signal is positive for D-Ala-D-Ala and L-Ala-D-Ala, and negative for L-Ala-L-Ala and D-Ala-L-Ala; thus the sign depends on the chirality of the carbon at the carboxylate end of the molecule. This means that the proximity of the chiral carbon is enough to produce a chiral perturbation, which can be detected for large signals.

CHAPTER VIII

VIBRATIONAL CIRCULAR DICHROISM OF AAMA.

As a part of the early work using the VCD technique we collected a series of spectra of N-acetyl-L-alanine-N'-acetamide, AAMA. This was done partly to demonstrate the ability of the instrument, and partly with the view of incorporating the results in the study of a series of molecules starting with alanine itself and going on to alanyl oligopeptides via alanyl-alanine, AAMA, and alanyl-alanyl-alanine. As so often happens the project was left unfinished as other problems caught the group's interest. Unfortunately, to attempt a thorough analysis now would be meaningless in light of the following developments:

1) The quality of spectra obtainable with the VCD instrument has been improved considerably, making it possible to get much better spectra, particularly in aqueous solutions, than was previously possible.

2) Another instrument has been built which works at its optimum in the amide I region, giving many times better signal to noise than was obtained previously in this region.

3) Petr Malon, a visiting professor from Czechoslovakia,

brought with him a series of analogous compounds which his group have studied extensively, using CD and proton NMR techniques (88).

The last development in particular would make any analysis attempted now premature. However, there is sufficient data available to make some comments.

Background.

As Figure 1 shows AAMA is in an interesting molecule in the context of the analysis of the conformations of peptides. It is the smallest molecule to possess two complete peptide linkages with complete torsional Φ and Ψ angles as defined for peptides (89), and yet it has aliphatic end groups, as opposed to the zwitterionic di- and tri-alanine. It may therefore be thought of as a piece in the middle of a peptide chain, as well as a molecule in its own right. Previous studies, including vibrational analysis, as well as electronic CD, proton NMR, and various calculations, have shown that AAMA exists in more than one conformation, and that the solvent used determines which conformer predominates. Thus, in an earlier vibrational study Avignon and Lascombe (90) found that the extended form of AAMA, also called the C_5, and the C_7 conformers both exist in dilute carbon tetrachloride, and that the C_7 conformer also occurs in aque-

A

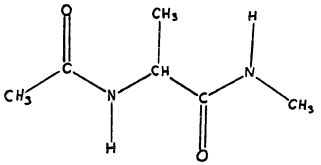

B

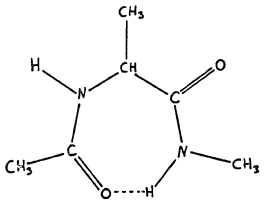

Figure 1. N-acetyl-L-alanine-N'-methylamide, AAMA, in two of its conformations:

A) C_5 conformer (extended form).

B) C_7 conformer.

ous solution. (Table I lists the torsional angles, ϕ and ψ, associated with the various conformers discussed here). In 1980 Madison and Kopple carried out a very thorough study of the acetyl-methylamides of alanine and proline, using solvents of increasing polarity (91). They drew the conclusion that as the polarity of the solvent increases the predominance of the C_7 conformer changes to an increasing population of the conformers α_R and P_{II}, both of which are dominant in aqueous solutions (the torsional angles of these conformers are in Table I). Recognizing the importance of the bulkiness of the side chain of the amino acid Malon and coworkers extended that study by examining the methyl amides of the following N-acetyl-a-amino acids: L-alanine, L-leucine, L-valine, L-tert-leucine, and L-proline (88). The increasing steric hindrance of the side chain reduces the flexibility of the molecule and therefore the number of possible conformers. Although largely in agreement with Madison they drew the conclusion that, while for AAMA the C_7 is present in all solvents used, the more polar solvents have a predominance of α_R and 3_{10} conformers (For torsional angles see Table I). Both Malon and Madison discussed the importance of solvent interaction (hydrogen bond formation) with the N-H groups (acetonitrile) only, and with both N-H group and C=O groups (aqueous solutions). The latter observation is a reminder that it is

Table I

Conformer	$\bar{\Phi}$	I	References
C_5	-120 to -150°	+ 150°	Madison & Kopple (91)
C_7	-80°	+80°	" "
P_{II}	-78°	+149°	Arnott & Dover (93)
α_R	-57°	-47°	Arnott & Dover (94)
3_{10}	-45°	-30°	Prasad & Sasisekheran (95)

$\bar{\Phi}$ and I of the various conformers of AAMA mentioned in the text. Avignon and Lascombe reported values of -60° and 40° for the C_7 conformer (90).

not possible to draw conclusions about aqueous solutions based on a scale of solvents of increasing polarity: water holds an unusual position because it can solvate both of the two sites just mentioned and because the interactions are facilitated by the small size of the water molecule.

Early Results.

It is evident from the above that a simple easily interpretable VCD spectrum of AAMA cannot be expected. Of the solvents used for the above studies the one which is most transparent in the IR and therefore suitable for VCD experiments is deuterated acetonitrile, CD_3CN. Fortunately, this is also the solvent most similar to water, both in terms of its polarity and in terms of the solution conformers it supports. A series of spectra were therefore collected of both deuterated and undeuterated AAMA in CD_3CN in the regions covering the amide I and III vibrations. Later data were also collected for AAMA in H_2O in the amide III region, and in D_2O in the amide I and III region. All spectra were collected with the instrument set with a fixed 2 mm slitwidth and a 1 s time constant. Ten scans of the solvent alone were collected and averaged, and subtracted from ten averaged scans of solvent and AAMA. Table II summarizes the results obtained, and the spectra are shown in Figure 2 - 4.

Table II

	Solvent	Conc.	Path	Freq. in cm^{-1}	IR intens. A	VCD intens. $\Delta A \cdot 10^6$
AmI	CD_3CN	0.1M	125μ	1687	0.70	-4.6
AmI'	CD_3CN	0.1M	125μ	1685	0.77	-6.3
AmI'	D_2O	1.2M	15μ	1634	0.55	-6.4
AmIII	CD_3CN	0.1M	600μ	1269	0.47	-24.2
	"	"	"	1296	0.36	+22.2
AmIII	H_2O	1.2M	15μ	1277	0.17	-5.6
	"	"	"	1314	0.21	+5.6
AmIII'	CD_3CN	0.1M	600μ	1265	0.16	-4.4
	"	"	"	1298	0.16	+16.1
AmIII'	D_2O	1.2M	25μ	- #	- #	- #
	"	"	"	1298	0.05	+7.7

IR and VCD intensities in the amide I and III regions in acetonitrile and aqueous solutions. #: The combination of the weakness of the signal and the high absorbance of the solvent in this region made these signals unreliable.

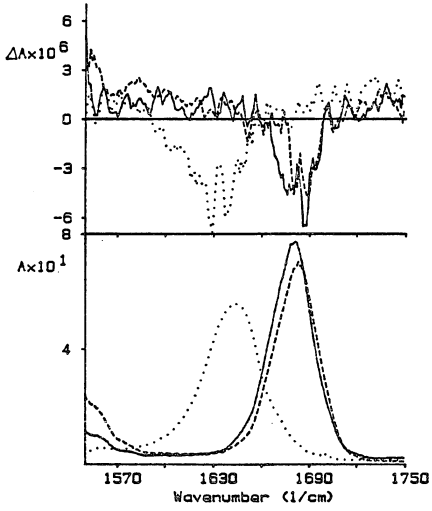

Figure 2. VCD spectra, top, and IR spectra, bottom, of the amide I region of AAMA, from 1550 - 1750 cm^{-1}. ——— AAMA in CD_3CN, ------- deuterated AAMA in CD_3CN, and ..... deuterated AAMA in D_2O. All VCD spectra presented after nine point smoothing.

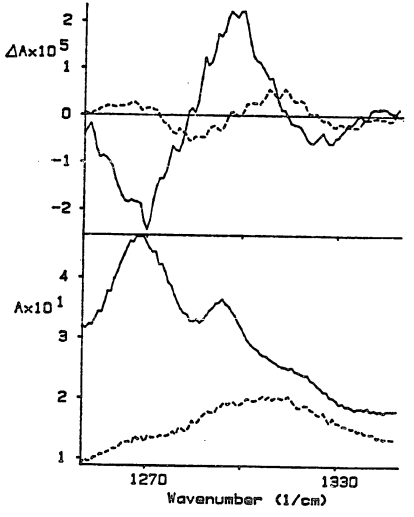

Figure 3. VCD spectra, top, and IR spectra, bottom, of the amide III region of AAMA, from 1250 - 1350 cm^{-1}. ——— AAMA in CD_3CN, and ------- AAMA in H_2O, the latter after five point smoothing.

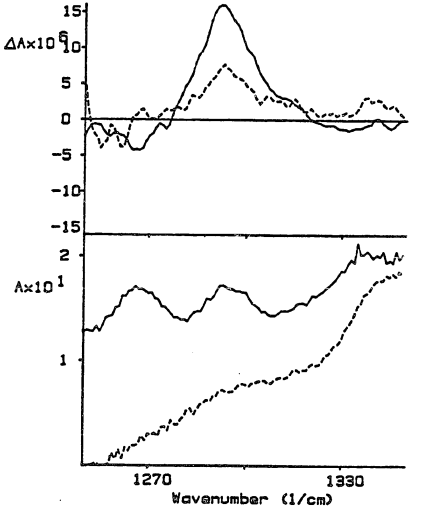

Figure 4. VCD spectra, top, and IR spectra, bottom, of the amide III' region of AAMA, from 1250 - 1350 cm^{-1}. ——— AAMA-Nd_1 in CD_3CN, and ------- deuterated AAMA-Nd_1 in D_2O, spectra of the latter after five point smoothing.

Discussion.

Amide I.

The amide I normal mode consists primarily of the carbonyl stretch (46) (see also chapter IV). According to the predictions of Schellman, and Holzwarth (9, 13) the degeneracy of this mode is lifted if the two carbonyl groups are in a dissymmetrical arrangement. In that case the resulting coupled oscillators give rise to a bisignate VCD signal, the magnitude of which depends on the geometrical arrangement of the two groups (See chapter V). This, however, only holds true if the molecule in question has a conformation which is stable on the time scale of the experiment. In the present case, where there are at least two different conformers, the signal observed is due to the overlapping signals of all the conformers. As in the case of electronic CD it may be possible to disentangle the overlapping signals, or the signal of one of the conformers may dominate the spectrum (88, 91). Figure 2 shows the spectra of the amide I region of AAMA, undeuterated in CD_3CN, and deuterated in CD_3CN and D_2O. As already mentioned it is now possible to get much better signal to noise in that region; nevertheless, it is obvious that the VCD signals are very similar in all three instances: in each case there is a small negative VCD signal, which shifts in the D_2O solu-

tion, due to deuterium bonding, as expected, but apart from that the signals are remarkably similar. Since there is no signal in the amide I region of alanyl-alanine the observed signals are almost certainly due to the kind of coupled oscillator mechanism referred to above. Thus the amide I signals indicate that the same conformer dominates in the CD_3CN and D_2O solutions and that deuteration of the labile protons has very little effect on the observed signals. As mentioned previously the spectrum of L-Ala-L-Ala-L-Ala, recorded by this group, shows a clear negative-positive amide I couplet from which has been deduced the most likely solution conformations of this tripeptide (63). It is therefore more than likely that the further analysis of this region of AAMA and similar compounds will yield information about the number and identity of the conformers, as well as the shape and size of their VCD signals. Such information will be important in the further understanding of VCD spectra of small peptides.

Amide III.

In view of the thorough study of alanyl-alanine already carried out the amide III region is naturally of special interest. It has been stated elsewhere (92) that the amide III region is sensitive to the identity of the amino acid, that is, to its side chain. It should there-

fore be particularly interesting to examine simultaneously the amide I and III regions of the methyl-acetamides mentioned in the beginning of this chapter, and perhaps compare them to the di- and tri-peptides of the corresponding amino acids.

Figure 3 shows the spectra of the amide III region of AAMA in H_2O and in CD_3CN. The VCD spectrum of the CD_3CN solution shows a clear negative-positive signal, corresponding in frequency to the IR signals. By contrast the signal to noise ratio in the aqueous sample was very poor and the VCD spectrum presented has been smoothed, but may in fact not be very reliable. It is presented primarily as a suggestion that CD_3CN may be a good choice of solvent when using water presents a problem. This is further supported by Figure 4 which shows the spectra of deuterated AAMA in D_2O and in CD_3CN. Although the signal to noise is poorer in the D_2O solution the spectra are similar. The single positive signal occurs at approximately the same frequency, which indicates that the effect of solvation of the N-D group is very similar in the two solvents. However, to properly understand this region of the AAMA spectrum it may be necessary to obtain the vibrational and VCD spectra of N-acetyl-L-Ala-d_1-N'-methylamide.

In spite of the incompleteness of data presented here,

there is little doubt that the upcoming VCD experiments, accompanied by appropriate calculations, will help to throw new light on the question of AAMA solution conformer, or to consolidate some of the results already obtained.

REFERENCES

(1) Applequist, J. American Scientist. 1987, 75, 59.

(2) Cotton, F. A. "Chemical Applications of Group Theory", Wiley-Interscience: New York, 1971; p 33.

(3) Hecht, E. "Optics", Addison-Wesley Publishing Company: Reading, 1988.

(4) Freedman, T. B.: Nafie, L. A. In "Topics in Stereochemistry"; Eliel, E. L.: Wilen, S. H., Eds.; John Wiley & Sons: New York, 1987; p 120.

(5) Keiderling, T. Appl. Spectrosc. Rev. 1981, 17, 189.

(6) Nafie, L. A.: Diem, M. J. Am. Chem. Soc. 1979, 12, 296.

(7) Deutsche, C. W.: Moscowitz, J. J.Chem. Phys. 1968, 49, 3257.

(8) Deutsche, C. W.: Moscowitz, J. J.Chem. Phys. 1970, 53, 2630.

(9) Schellman, J. A. J. Chem. Phys. 1973, 58, 2882.

(10) Schellman, J. A. J. Chem. Phys. 1974, 60, 343.

(11) Snir, J.: Frankel, R. A.: Schellman, J. A. Biopolymers. 1975, 14, 173.

(12) Schellman, J. A. In "Peptides, Polypeptides and Proteins"; Blout, E. R.: Bovey, F. A.: Goodman, M.:

Nolan, N., Eds.; Wiley: New York, 1974; p 320.

(13) Holzwarth, G.: Chabay, I. J. Chem. Phys. 1972, 57, 1632.

(14) Tinoco, I. Jr. Radiation Res. 1963, 20, 133.

(15) Diem, M.: Roberts, G. M.: Lee, O.: Barlow, A. Appl. Spectrosc. 1988, 42, 20.

(16) Grosjean, M.: Legrand, M. C. R. Sci. (Paris) 1960, 251, 2150.

(17) Velluz, L.: Grosjean, M.: Legrand, M. "Optical Circular Dichroism"; Academic Press: New York, 1965.

(18) Cheng, J. C.: Nafie, L. A.: Allen, S.D.: Braunstein, A.I. Appl. Opt. 1976, 15, 1960.

(19) Schrader, B.: Korte, E. H. Angew. Chem. 1972, 84, 218.

(20) Chabay, I. Chem. Phys. Lett. 1972, 17, 283.

(21) Dudley, R. J.: Mason, S. F.: Peacock, R. D. J. Chem. Soc., Chem. Commun. 1972, 1084.

(22) Holzwarth, G.: Chabay, I.: Holzwarth, N. A. W. J. Chem. Phys. 1973, 58, 4816.

(23) Hsu, E. C.: Holzwarth. G. J. Chem. Phys. 1973, 59, 4678.

(24) Holzwarth, G.: Hsu, E. C.: Mosher, H. S.: Faulkner, T. R.: Moscowitz, A. J. Am. Chem. Soc. 1974, 96, 251.

(25) Nafie, L. A.: Cheng, J. C.: Stephens, P. J. J. Am. Chem. Soc. 1975, 97, 3842.

(26) Nafie, L. A.: Keiderling, T. A.: Stephens, P. J. J.

Am. Chem. Soc. 1976, 98, 2715.

(27) Keiderling. T. A.: Stephens. P. J. Chem. Phys. Lett. 1976, 41, 46.

(28) Diem, M.: Polavarapu, P. L.: Oboodi, M.: Nafie, L. A. J. Am. Chem. Soc. 1982, 104, 3329.

(29) Oboodi, M. R.: Alva, C.: Diem, M. J. Phys. Chem. 1984, 88, 501.

(30) Live, D. H.: Agosta, W. C.: Cotburn, D. J. Org. Chem. 1973, 42, 3356.

(31) Greenstein, J.P.: Winitz, M. In "Chemistry of the Amino Acids"; Wiley-Interscience: New York, 1961, Vol. 3, p 1831.

(32) Moroder, L.: Hallett A.: WÜnsch, E.: Keller, O.: Wersin, G.: Hoppe-Seyler's Z. Physiol. Chem. 1976, 357, 1651.

(33) Gisin, B. F. Helv. Chim. Acta. 1973, 56, 1476.

(34) Kaiser, E.: Colescott, R. L.: Bossinger, C. D.: Cook, P. I. Anal. Biochem. 1970, 34, 595.

(35) Troll, W.: Cannan, R. K. J. Biol. Chem. 1953, 200, 803.

(36) Bodanszky, M.: Klausner, Y. S.: Ondetti, M. A. "Peptide Synthesis"; Wiley: New York, 1976, p 167.

(37) Levine, I. N. "Quantum Chemistry"; Allyn & Bacon, Inc.: Boston, 1983.

(38) Murrell, J. N.: Kettle, S. F. A.: Tedder, J. M.

"Valence Theory"; John Wiley & Sons Ltd.: New York, 1965.

(39) Wilson, E. B.: Decius, J. C.: Cross, P. C. "Molecular Vibrations"; Dover Publications, Inc.: New York, 1980.

(40) Schachtschneider, J. H.

a)"Vibrational Analysis of Polyatomic Molecules. V."

b)"Vibrational Analysis of Polyatomic Molecules. VI."; Emeryville, CA, 1964, Shell Development Company Report, p 231-264.

(41) Diem, M.: Barlow, A. J. Chem. Ed., in press.

(42) Urey, H. C.: Bradley C. A. Phys. Rev. 1931, 38, 1969.

(43) Simanouti, T. J. Chem. Phys. 1949, 17, 245.

(44) Lord, R. C. Appl. Spectrosc. 1977, 31, 187.

(45) Thomas, G.J., Jr. In "Vibrational Spectra and Structure"; Durig, J., Ed.; 1975, Vol. III.

(46) Miyazawa, T.: Shimanouchi, T.: Mizushima, S. J. Chem. Phys. 1958, 29, 611.

(47) Roberts, G. M.: Lee, O.: Callienni, J.: Diem, M. J. Am. Chem. Soc. 1988, 110, 1749.

(48) Gupta, M. K.: Gupta, V. D. Indian J. Biochem. Biophys. 1978, 15, 413.

(49) Callienni, J.: Trager, J. B.: Davies, M. A.: Gunnia, U.: Diem, M. J. Phys. Chem. 1989, 93, 5049.

(50) Nafie, L. A.: Diem, M. Acc. Chem. Res. 1979, 12, 296.

(51) Michel, J.: Thulstrup, E. W. "Spectroscopy with Polarized Light"; VCH Publishers: New York, 1986; Chapter I.

(52) Stephens, P. J.: Lowe, M. A. Ann. Rev. Phys. Chem. 1985, 36, 213.

(53) Cohan, N. V.: Hameka, H. F. J. Am. Chem. Soc. 1966, 88, 2136.

(54) Abbate, S.: Laux, L.: Overend, J.: Moscowitz, A. J. Chem. Phys. 1981, 75, 609.

(55) Polavarapu, P. L. Mol. Phys. 1983, 49, 645.

(56) Barnett, C. J.: Drake, A. F.: Kuroda, R.: Mason, S. F. Mol. Phys. 1980, 41, 455.

(57) Barron, L.D.: Buckingham, A. D. J. Am. Chem. Soc. 1979, 101, 1979.

(58) Freedman, T. B.: Balukjian, G. A.: Nafie, L. A. J. Am. Chem. Soc. 1985, 107, 6213.

(59) Nafie, L. A.: Walnut, T. H. Chem. Phys. Lett. 1977, 49, 441.

(60) Walnut, T. H.: Nafie, L. A. J. Chem. Phys. 1977, 67, 1501.

(61) Freedman. T. B.: Nafie, L. A. J. Chem. Phys. 1983, 78, 645.

(62) Stephens, P. J. J. Chem. Phys. 1985, 89, 748.

(63) Lee, O.: Roberts, G. M.: Diem, M. Biopolymers, 1989, 28, 1759.

(64) Gulotta, M.: Goss, D. J.: Diem, M. Biopolymers, 1989, 28, 2047.

(65) Diem, M.: Lee, O.: Roberts, G. M., submitted for publication in J. Am. Chem. Soc.

(66) Kauzman, W. "Quantum Chemistry: An Introduction"; Academic Press: New York, 1957; p 504.

(67) Moscowitz, A. "Modern Quantum Chemistry"; Sinanoğlu, O. Ed.; Academic Press: New York, 1966; Vol. III.

(68) Dirac, P. A. M. "Quantum Mechanics", 4th ed.; Oxford University Press: London, 1958.

(69) Keiderling, T. A.: Stephens, P. J. J. Am. Chem. Soc. 1978, 99, 8061.

(70) Narayanan, U.: Keiderling, T. A. J. Am. Chem. Soc. 1983, 105, 6406.

(71) Faulkner, T. R. Ph. D. Dissertation, University of Minnesota, 1976.

(72) Nafie, L. A.: Diem, M. Appl. Spectrosc. 1979, 33, 130.

(73) Nafie, L. A.: Diem, M.: Vidrine, D. W. J. Am. Chem. Soc. 1979, 101, 496.

(74) Lipp, E. D.: Nafie, L. A.: Appl. Spectrosc. 1984, 38, 20.

(75) Polavarapu, P. L. Appl. Spectrosc. 1984, 38, 26.

(76) Levinstein, H. Phys. Today, Nov. 1977, 23.

(77) Data supplied with HgCdTe detector from IR Associ-

ates.

(78) Singh, R. D.: Keiderling, T. A. Biopolymers; 1981, 20, 237.

(79) Lal, B. B.: Nafie, L. A. Biopolymers, 1982, 21, 2161.

(80) Sen, A. C.: Keiderling, T. A. Biopolymers, 1984, 23, 1519.

(81) Sen, A. C.: Keiderling, T. A. Biopolymers, 1984, 23, 1537.

(82) Narayanan, U.: Keiderling, T. A.: Bonora, G. M.: Toniolo, C. Biopolymers, 1985, 24, 1257.

(83) Narayanan, U.: Keiderling, T. A.: Bonora, G. M.: Toniolo, C. J. Am. Chem. Soc. 1986, 108, 2431.

(84) Yasui, S. C.: Keiderling, T. A. J. Am. Chem. Soc. 1986, 108, 5576.

(85) Paterlini, G. M.: Freedman, T. B.: Nafie, L. A. Biopolymers 1986, 25, 1751.

(86) Diem, M. J. Am. Chem. Soc. 1988, 110, 6967.

(87) "CRC Handbook of Chemistry and Physics"; Weast, R. C.: Lide, D. R.: Astle, M. J.: Beyer, W. H.; CRC Press: Florida, 1989.

(88) Malon, P.: Pancoska, P.: Budesinsky, M.: Hlavacek, J.: Pospisek, J.: Blaha, K. Coll. Czech. Chem. Comm. 1983, 48, 2844.

(89) IUPAC - IUB Commission on Biochemical Nomenclature,

Biochemistry, 1970, 18, 3471.

(90) Avignon, M.: Lascombe, J. Jerusalem Symp. Quantum Chem. Biochem. 1973, 5, 97.

(91) Madison, V.: Kopple, K. D. J. Am. Chem. Soc. 1980, 102, 4855.

(92) Hsu, S. L.: Moore, W. H.: Krimm, S.Biopolymers, 1976, 15, 1513.

(93) Arnott, S.: Dover, S. D. J. Mol. Biol. 1967, 30, 209.

(94) Arnott, S. Dover, S. D. Acta Cryst. 1968, B24, 599.

(95) Prasad, B. V. V.: Sasisekharan, V. Macromolecules, 1979, 12, 1107.